A sample of 6C radio sources designed to find objects at redshift > 4: II — spectrophotometry and emission line properties

Matt J. Jarvis[1,2*], Steve Rawlings[1], Mark Lacy[1,3,4], Katherine M. Blundell[1],
Andrew J. Bunker[5,6], Steve Eales[7], Richard Saunders[8], Hyron Spinrad[6],
Daniel Stern[6,9] and Chris J. Willott[1]

[1] *Astrophysics, Department of Physics, Keble Road, Oxford, OX1 3RH, UK*
[2] *Sterrewacht Leiden, Postbus 9513, 2300 RA Leiden, the Netherlands*
[3] *Institute of Geophysics and Planetary Physics, L-413 Lawrence Livermore National Laboratory, Livermore, CA 94550, USA*
[4] *Department of Physics, University of California, 1 Shields Avenue, Davis CA 95616, USA*
[5] *Institute of Astronomy, University of Cambridge, Madingley Road, Cambridge CB3 0HA, UK*
[6] *Astronomy Department, University of California at Berkeley, CA 94720*
[7] *Department of Physics and Astronomy, University of Wales College of Cardiff, P.O. Box 913, Cardiff, CF2 3YB, UK*
[8] *Astrophysics Group, Cavendish Laboratory, Madingley Road, Cambridge CB3 0HE, UK*
[9] *Jet Propulsion Laboratory, California Institute of Technology, Mail Stop 169-327, Pasadena, CA 91109*

7 January 2007

ABSTRACT

This is the second in a series of three papers which present and interpret basic observational data on the 6C* 151-MHz radio sample: a low-frequency selected sample which exploits filtering criteria based on radio properties (steep spectral index and small angular size) to find radio sources at redshift $z > 4$ within a 0.133 sr patch of sky. We present results of a programme of optical spectroscopy which has yielded redshifts in the range $0.5 \lesssim z \lesssim 4.4$ for the 29 sources in the sample, all but six of which are secure. We find that the filtering criteria used for 6C* are very effective in excluding the low-redshift, low-luminosity radio sources: the median redshift of 6C* is $z \approx 1.9$ compared to $z \approx 1.1$ for a complete sample matched in 151-MHz flux density. By combining the emission-line dataset for the 6C* radio sources with those for the 3CRR, 6CE and 7CRS samples we establish that $z \geq 1.75$ radio galaxies follow a rough proportionality between Lyα- and 151 MHz-luminosity which, like similar correlations seen in samples of lower-redshift radio sources, are indicative of a primary link between the power in the source of the photoionising photons (most likely a hidden quasar nucleus) and the power carried by the radio jets. We argue that radio sources modify their environments and that the range of emission-line properties seen is determined more by the range of source age than by the range in ambient environment. The smallest $z > 1.75$ radio galaxies have all the properties expected if the size distribution of luminous high-redshift steep-spectrum radio sources reflects a broad range (~ 2 dex) of source ages with a narrower range ($\lesssim 1.5$ dex) of environmental densities, namely: (1) high-ionisation lines, e.g. Lyα, of relatively low luminosity; (2) boosted low-ionisation lines, e.g. CII]; (3) spatially compact emission-line regions; and (4) HI-absorbed Lyα profiles. This is in accord with the idea that all high-redshift, high-luminosity radio sources are triggered in similar environments, presumably recently collapsed massive structures.

Key words: radio continuum: galaxies - galaxies: active - galaxies: emission lines

1 INTRODUCTION

Observations of active galaxies provide a relatively straightforward way of probing conditions within mas-

---

* Email: jarvis@strw.leidenuniv.nl

sive structures in the young Universe, and may play an important role in placing constraints on cosmological models for structure formation. Radio galaxies are particularly useful in this respect as their optical and infra-red emission tend not to be dominated by an active nucleus as is the case for quasars, hence the structural properties of their host galaxies are less difficult to determine. The general belief that powerful radio galaxies harbour hidden quasar nuclei leads to another advantage of using radio galaxies as cosmological probes: the hidden nuclei and/or shocks associated with jets can excite strong narrow emission lines, making redshift determination much easier than is afforded by the relatively weak absorption lines of 'normal' massive elliptical galaxies.

Radio galaxies at redshifts $z > 4$ provide information on the Universe at an epoch $\lesssim 10^9$ years ($\Omega_M = 1$ and $\Omega_\Lambda = 0$, $H_\circ = 50$ km s^{-1} Mpc^{-1}) after the Big Bang. The principal difficulties involved in finding high-redshift radio sources from flux-density-limited samples have been highlighted previously (e.g. Blundell et al. 1998). Such objects are absent from the brightest radio samples (e.g. the 3CRR sample: Laing, Riley & Longair 1983) because of what is effectively an upper limit to the low-frequency radio luminosity of radio galaxies. However, such luminous sources could be detected up to very high redshift in fainter (151-MHz flux-density, $S_{151} \approx 1$ Jy) flux-density limited samples, for example the most radio luminous 3CRR source (3C9) could in principle be detected out to $z \sim 10$ in a 1 Jy sample. If luminous radio sources were present at this epoch, they have not been detected so far. One reason for this is the rapid decrease in the fraction of high-luminosity, high-redshift radio sources as the flux-density limit of the sample is reduced. This means that compiling redshift complete flux-density-limited samples with a significant number of high-redshift sources over moderate sky areas becomes extremely difficult. Indeed, at $S_{151} \sim 1$ Jy, the source count is $\sim 10^4$ per steradian, and even in the absence of a decline in the co-moving space density of such sources at high redshift (c.f. Dunlop & Peacock 1990; Willott et al. 2001a; Jarvis et al. 2001a), we would not expect to find more than $\approx 1\%$ of these sources at $z > 4$.

To ameliorate the problem of the increasing source counts at faint flux-density, various groups have employed additional filtering criteria to find high-redshift radio sources. The most widely used is the steep spectral index criterion [e.g. Chambers, Miley & van Breugel (1990); Röttgering et al. (1994); Lacy et al. 1994; Chambers et al. (1996)], which utilises the steep and often curved radio spectra of many radio-luminous sources. The correlations between radio luminosity, redshift and spectral shape are rather complicated (see e.g. Blundell, Rawlings & Willott 1999) but the simplest effects to appreciate are: (i) that the spectral index measured for a source at high redshift will be steeper than the same source observed at a lower redshift if, as is typically the case, that source has a concave radio spectrum; (ii) more luminous sources tend to have steeper spectra above frequencies at which absorption effects become important. Filtering based on steep radio spectra is one of the selection criteria used to filter the 6C* sample which was defined in Blundell et al. (1998).

A second filtering criterion used is an angular size limit. This criterion has been used because sources at high redshift are intrinsically smaller than those at low-redshift in the same flux-density-limited sample. (e.g. Neeser et al. 1995; Blundell et al. 1999). The physical cause of this 'linear size evolution' has been the cause of recent debate: Neeser et al. (1995) suggested that the environments of radio galaxies change systematically with epoch, while Blundell et al. (1999) argued that the sources are shorter because they are observed when they are younger [c.f. Kaiser, Dennett-Thorpe & Alexander (1997) and Blundell & Rawlings (1999)].

The 6C* sample was devised to provide a filtered sample biased towards detecting radio galaxies at $z > 4$ within a sample of spectroscopic targets that was small enough that complete redshift information could conceivably be obtained. The 6C* sample led to the discovery of one of the highest redshift radio sources currently known (6C*0140+326 at $z = 4.41$; Rawlings et al. 1996) and more recently it has been used to place constraints on the radio luminosity function of the most-luminous radio-loud objects at high redshift, thus placing constraints on the evolution in the co-moving space density of these sources (Jarvis et al. 2001a).

In this paper we present the optical spectroscopy of the 6C* sample. In Sec. 2 we outline the properties of the 6C* sample, and an appendix gives brief notes on sources in the original 6C* list (Blundell et al. 1998) but which are now excluded. In Sec. 3 we outline the observational techniques employed and present the optical spectra for 28 of the 29 sources remaining in the sample, giving notes on each source in Sec. 4. In Sec 5 we investigate the redshift space probed by 6C* and compare it to the distribution of sources one might find in a sample without the filtering criteria but at the same limiting flux-density as 6C*. In Sec. 6 we combine the 6C* spectrophotometric dataset with similar datasets from the 3CRR sample (see summary in Willott et al. 1999), 6CE (Rawlings, Eales & Lacy 2001) and 7CRS (Willott et al. in prep; Blundell et al. in prep) samples to investigate how various optical properties of high-redshift radio sources are linked to their radio properties. In Sec. 7 we seek to explain the results of Sec 6 in terms of a simple physical model for radio source evolution.

Our spectroscopic programme on the 6C* sample has been supplemented by imaging data (principally in the $K-$band) taken throughout the past decade. In many cases, the spectroscopic observations which have led to the spectra shown in this paper have used iden-

tifications based on these data. We defer presentation of the imaging data (principally in R- and K-bands) on the 6C* sample to the final paper in this series (Jarvis et al. 2001b; hereafter Jea01).

We use $H_\circ = 50 \, \mathrm{km \, s^{-1} \, Mpc^{-1}}$, $\Omega_M = 1$ and $\Omega_\Lambda = 0$ throughout; none of the principal results are sensitive to this particular choice of cosmological parameters. Radio flux-density is measured in Jy, all radio luminosities quoted are measured in units of $\mathrm{W \, Hz^{-1} \, sr^{-1}}$, and the convention for radio spectral index (α) is that $S_\nu \propto \nu^{-\alpha}$, where S_ν is the flux-density at frequency ν. Narrow-line luminosities are measured in units of W.

2 THE 6C* SAMPLE

The selection criteria used to filter the 6C* sample, discussed fully in Blundell et al. (1998), are summarised as follows:

- $00^{\mathrm{h}}20^{\mathrm{m}} \leq$ R.A. (B1950) $\leq 02^{\mathrm{h}}10^{\mathrm{m}}$
- $30° \leq$ Dec. (B1950) $\leq 51°$
- $0.96 \, \mathrm{Jy} \leq S_{151} \leq 2.00 \, \mathrm{Jy}$
- $\alpha_{151}^{4850} \geq 0.981$, where α_{151}^{4850} is the radio spectral index measured between 151 MHz and 4850 MHz.
- $\theta_{\mathrm{Texas}} < 15''$, where θ_{Texas} is the angular size of the radio source given in the Texas catalogue of radio sources at 365 MHz (Douglas et al. 1996).

These selection criteria resulted in the original 6C* sample comprising 34 objects. Further radio information obtained either from the NVSS catalogue (Condon et al. 1998) or from our own subsequent radio observations have led to five of these objects being identified as having an angular size larger than 15 arcsec, and these are now excluded from the sample. Notes and data on these five excluded sources can be found in Appendix A. Therefore, the 6C* sample now comprises 29 sources. In 23 cases (80%) the spectroscopic redshifts are unequivocal, in 6 (20%) further spectroscopic confirmation is ideally required, although tentative redshifts are given; these are normally based on a single definite emission line identified with a specific feature on the basis of a redshift estimate from the $K-$band magnitude.

3 THE OBSERVATIONS

The optical spectra presented in this paper were obtained from many observing runs on three different telescopes. The vast majority of the redshifts for this sample were obtained using spectra taken on four runs at the WHT, from January 1991 using the FOS-II spectrometer, and on three occasions up until February 2000 using the red- and blue-arms of the ISIS spectrometer. Spectra for four of the fainter sources were obtained using the low resolution imaging spectrometer on the Keck-II telescope between August 1998 and October 1998. Further spectroscopy on the Lick-3m telescope in October

1998 allowed us to confirm redshifts for those sources lacking a secure redshift from the WHT observations. A summary of all of these observations is presented in Table 1. The observations were carried out by offsetting from bright stars to either the radio position, or to where there was an identification based on our R- or K-band imaging (Jea01). The position angle (PA) of the slit was aligned with the radio structure in the cases where there was only one or no infrared counterpart. Otherwise, the PA was oriented to pass through the two most probable counterparts. For presentation purposes most of the spectra have been boxcar smoothed over three pixels. The measurements presented in Table 2 were all made prior to this smoothing process. Reduction of the spectra was carried out using standard IRAF routines. The one-dimensional spectra were extracted from the two-dimensional data with two apertures: a full-width at zero-intensity for flux measurement purposes, and a full-width at half-maximum for good signal-to-noise. Cosmic rays were edited out of the 1-D spectra by inspection of the 2-D spectra and in all cases, apart from the single-arm observations on the Keck telescope, the spectra from the red and blue arms were joined together by averaging over $\approx 50 \, \text{Å}$ in the overlapping regions.

For the pre-1998 WHT+ISIS observations the beam was split using the 540 nm dichroic; the blue-arm detector was the TEK1 chip on all runs up until and including 1995 and the EEV12 chip on all runs later than 1995 with pixel scales of 0.358 and 0.2 arcsec pixel^{-1} respectively; the red-arm detector was the EEV3 chip in 1994 and the TEK2 chip from 1995 with pixel scales of 0.336 and 0.358 arcsec pixel^{-1} respectively. For the post-1998 runs the dichroic used split the beam at 610 nm. The spectra taken on the Keck-II telescope with LRIS (Oke et al. 1995) used a TEK 2048×2048 CCD detector with a pixel scale of 0.212 arcsec pixel^{-1}; we used a 300 lines/mm grating which has a spectral scale of 2.44 Å pixel^{-1} at a central wavelength of $\approx 6500 \, \text{Å}$. For the Lick-3m observations the observations were made using the Kast double spectrograph (Miller & Stone 1994) with a Reticon 400×1200 CCD detector for both blue- and red-arms. For the blue-arm the 452/3306 grating was used which gives a spectral scale of 2.54 Å pixel^{-1}, and the 300/7500 grating was used for the red-arm observations giving a spectral scale of 4.60 Å pixel^{-1}.

In nearly all of the cases, definite emission lines have been detected and in all of the others plausible emission lines are seen. The reduced 1-D spectra are presented in Fig. 2.

Source name	Pointing Position B1950		Telescope + Spectrometer	Date	Exposure time (s)	Slit width (arcsec)	PA (°)
6C*0020+440	**00 20 01.70**	**+44 02 32.1**	**WHT+ISIS**	**94Jan08**	**1800**	**3.0**	80
6C*0024+356	00 24 12.68	+35 39 47.7	Lick-3m+KAST	98Oct20	1200	2.0	106
	00 24 12.97	**+35 39 48.1**	**WHT+ISIS**	**98Dec20**	**1800**	**2.5**	**85**
6C*0031+403	00 31 46.85	+40 19 25.0	WHT+FOS-2	91Jan17	1200	4.0	90
	00 31 46.82	+40 19 25.9	WHT+ISIS	95Jan29	2700	3.1	110
	00 31 46.82	+40 19 25.9	Lick-3m+KAST	98Oct20	2700	2.0	128
	00 31 46.82	**+40 19 25.9**	**WHT+ISIS**	**98Dec20**	**1800**	**2.5**	**128**
6C*0032+412	**00 32 10.73**	**+41 15 00.2**	**WHT+FOS-2**	**91Jan17**	**1200**	**4.0**	**128**
6C*0041+469	**00 41 16.04**	**+46 58 27.3**	**WHT+ISIS**	**95Jan29**	**1800**	**2.7**	**10**
	00 41 16.00	+46 58 25.3	Keck-II+LRIS	98Oct16	2400	1.0	171
6C*0050+419	00 50 46.52	+41 58 45.3	WHT+FOS-2	91Jan17	900	4.0	31
	00 50 46.90	**+41 58 46.7**	**Keck-II+LRIS**	**98Aug26**	**3600**	**1.0**	**41**
	00 50 46.50	+41 58 45.3	WHT+ISIS	00Feb09	1800	2.0	160
6C*0052+471	00 52 09.59	+47 09 46.2	WHT+FOS-2	91Jan17	900	4.0	12
	00 52 09.60	**+47 09 46.5**	**WHT+ISIS**	**95Jan28**	**900**	**3.1**	**10**
6C*0058+495	**00 58 24.75**	**+49 34 04.3**	**WHT+ISIS**	**92Jan28**	**900**	**4.0**	**35**
6C*0106+397	**01 06 35.31**	**+39 44 02.8**	**Keck-II+LRIS**	**98Aug25**	**3000**	**1.0**	128
6C*0112+372	01 12 00.33	+37 16 41.4	WHT+FOS-2	91Jan16	1200	4.0	108
	01 12 00.33	**+37 16 41.4**	**Lick-3m+KAST**	**98Oct20**	**2400**	**2.0**	**112**
6C*0115+394	01 15 03.47	+39 28 45.9	Lick-3m+KAST	98Oct20	5400	2.0	167
	01 15 03.47	**+39 28 45.9**	**WHT+ISIS**	**98Dec18**	**1800**	**2.5**	**166**
6C*0118+486	01 18 16.49	+48 41 58.0	WHT+FOS-2	91Jan17	600	4.0	150
	01 18 16.50	**+48 41 58.1**	**WHT+ISIS**	**95Jan28**	**900**	**0.9**	**155**
6C*0122+426	01 22 56.80	+42 36 16.0	Lick-3m+KAST	98Oct21	3600	2.0	85
	01 22 56.80	**+42 36 16.0**	**WHT+ISIS**	**98Dec17**	**1800**	**2.5**	**98**
6C*0128+394	01 28 34.70	+39 27 32.0	WHT+ISIS	95Jan28	900	0.9	20
	01 28 34.67	**+39 27 32.0**	**WHT+ISIS**	**98Dec20**	**1800**	**2.5**	**17**
6C*0132+330	**01 32 39.09**	**+33 01 40.4**	**WHT-ISIS**	**98Dec18**	**1800**	**2.5**	**174**
6C*0133+486	01 33 36.29	+48 37 07.9	WHT+ISIS	98Dec17	1800	2.5	24
	01 33 36.29	**+48 37 07.9**	**WHT+ISIS**	**98Dec19**	**2700**	**2.5**	**24**
6C*0135+313	**01 35 16.13**	**+31 17 27.3**	**WHT+ISIS**	**98Dec19**	**1800**	**2.5**	**67**
6C*0136+388	01 36 59.09	+38 48 09.2	WHT+FOS-2	91Jan16	2700	4.0	124
	01 36 59.31	+38 48 07.3	WHT+ISIS	95Jan29	1800	0.5	131
	01 36 59.09	**+38 48 09.5**	**WHT+ISIS**	**98Dec20**	**1800**	**2.5**	**132**
6C*0139+344	01 39 25.87	+34 27 02.5	WHT+ISIS	92Jan29	900	4.0	159
	01 39 25.85	+34 27 03.2	WHT+ISIS	95Jan28	900	0.9	155
	01 39 25.91	**+34 26 32.5**	**Keck-II+LRIS**	**98Sep04**	**3600**	**1.0**	**26**
6C*0140+326	**01 40 51.53**	**+32 38 45.8**	**WHT+ISIS**	**94Jan08**	**1200**	**2.0**	**128**
6C*0142+427	01 42 28.13	+42 42 41.6	WHT+FOS-2	91Jan17	1200	4.0	37
	01 42 28.14	**+42 42 41.9**	**WHT+ISIS**	**94Jan08**	**1800**	**3.0**	**37**
6C*0152+463	01 52 38.22	+46 22 30.4	WHT+ISIS	94Jan08	1800	3.0	0
	01 52 38.10	**+46 22 28.2**	**WHT+ISIS**	**95Jan28**	**900**	**3.1**	**30**
6C*0154+450	**01 54 24.85**	**+45 03 46.4**	**WHT+FOS-2**	**91Jan17**	**300**	**4.0**	**180**
6C*0155+424	01 55 29.74	+42 25 38.2	WHT+ISIS	94Jan08	1800	3.0	0
	01 55 29.74	**+42 25 38.2**	**WHT+ISIS**	**98Dec18**	**1800**	**2.5**	**102**
6C*0158+315	01 58 01.53	+31 31 45.7	WHT+ISIS	98Dec19	1800	3.0	169
	01 58 01.53	**+31 31 45.7**	**WHT+ISIS**	**98Dec20**	**3600**	**3.0**	**169**
6C*0201+499	02 01 08.41	+49 54 38.1	WHT+FOS-2	91Jan17	1500	4.0	178
	02 01 08.39	**+49 54 38.5**	**WHT+ISIS**	**95Jan28**	**1315**	**0.9**	**158**
6C*0202+478	02 02 07.03	+47 51 42.2	Lick-3m+KAST	98Oct21	1200	2.0	86
	02 02 06.90	**+47 51 41.70**	**WHT+ISIS**	**98Dec19**	**1800**	**2.5**	**83**
6C*0208+344	02 08 55.47	+34 29 57.3	WHT+FOS-2	91Jan17	1200	4.0	131
	02 08 55.50	**+34 29 57.0**	**WHT+ISIS**	**94Jan09**	**1800**	**3.0**	**120**
6C*0209+276	02 09 20.01	+47 39 16.6	WHT+ISIS	94Jan09	1800	3.0	0
	02 09 20.00	**+47 39 16.5**	**WHT+ISIS**	**00Jan11**	**1800**	**2.0**	**90**

Table 1: Log of the observations of the sources present in the 6C* sample. The larger, bold text represents the observation for the spectra presented in Fig. 2. The observations of 6C*0140+326 are detailed in Rawlings et al. (1996).

Source name	z	Line	λ_{rest} (Å)	λ_{obs} (Å)	FWHM (km s^{-1})	Flux (Wm^{-2})	Galaxy or Quasar
6C*0020+440	2.988	Lyα	1216	4850 ± 1	$600 - 1300$	3.4E-19 $\pm$ 25%	G
6C*0024+356	2.161	Lyα	1216	3844 ± 2	$0 - 1100$	2.8E-19 $\pm$ 10%	G
		CII]	2326	7356 ± 1	$800 - 1100$	1.4E-19 $\pm$ 15%	
6C*0031+403	1.619	CIV	1549	4057 ± 2	$0 - 1000$	8.7E-20 $\pm$ 10%	G
		CIII]	1909	4999 ± 1	$0 - 700$	4.4E-20 $\pm$ 10%	
6C*0032+412	3.658	Lyα	1216	5660 ± 1	$1000 - 1400$	2.1E-19 $\pm$ 10%	G
		CIV	1549	7194 ± 5	$1000 - 1300$	3.2E-20 $\pm$ 20%	
6C*0041+469	2.140?	Lyα?!	1216	3836 ± 12	$1000 - 1600$	1.1E-19 $\pm$ 20%	G
		CIV?!	1549	4872 ± 1	$0 - 900$	7.8E-20 $\pm$ 10%	
6C*0050+419	1.748?	HeII?	1640	4507 ± 1	$0 - 1000$	7.2E-21 $\pm$ 15%	G
		CII]?!	2326	6385 ± 2	$0 - 300$	4.2E-21 $\pm$ 10%	
		[NeIV]?	2424	6657 ± 3	$0 - 900$	8.1E-21 $\pm$ 15%	
6C*0052+471	1.935	Lyα	1216	3577 ± 8	> 2500	5.1E-19 $\pm$ 15%	Q
		CIV	1549	4549 ± 18	> 7000	1.1E-18 $\pm$ 60%	
		CIII]	1909	5599 ± 10	> 2500	3.7E-19 $\pm$ 35%	
6C*0058+495	1.173	CIII]	1909	4142 ± 7	$2000 - 2500$	4.1E-19 $\pm$ 15%	G
		CII]	2326	5034 ± 2	$1100 - 1600$	2.1E-19 $\pm$ 25%	
		MgII	2799	6087 ± 2	$800 - 1200$	2.1E-19 $\pm$ 20%	
		[OII]	3727	8097 ± 1	$800 - 1100$	1.0E-18 $\pm$ 10%	
		[SII]	4072	8863 ± 1	$600 - 900$	4.0E-19 $\pm$ 15%	
6C*0106+397	2.284	CIV	1549	5089 ± 2	$900 - 1300$	$>$ 2.0E-20	G
		HeII	1640	5384 ± 1	$300 - 900$	$>$ 2.7E-20	
		CIII]	1909	6262 ± 1	$300 - 700$	$>$ 1.8E-20	
6C*0112+372	2.535	Lyα	1216	4299 ± 1	$1400 - 1800$	1.6E-18 $\pm$ 15%	G
		CIV	1549	5476 ± 1	$350 - 900$	3.3E-19 $\pm$ 5%	
6C*0115+394	2.241	Lyα	1216	3940 ± 1	$700 - 1400$	4.0E-18 $\pm$ 10%	G
		CIV	1549	5020 ± 1	$0 - 1100$	2.7E-19 $\pm$ 15%	
		HeII	1640	5319 ± 2	$1000 - 1500$	3.4E-19 $\pm$ 25%	
		CIII]	1909	6193 ± 1	< 1800	2.1E-19 $\pm$ 15%	
		[NeIV]	2424	7861 ± 1	$0 - 700$	1.8E-20 $\pm$ 20%	
6C*0118+486a	2.350	Lyα	1216	4073 ± 1	$600 - 1300$	3.7E-19 $\pm$ 25%	G
		CIV	1549	5200 ± 2	$1200 - 1600$	1.5E-19 $\pm$ 20%	
6C*0118+486b	0.529	[OII]	3727	5702 ± 1	$0 - 800$	1.5E-19 $\pm$ 15%	G
		Hβ	4861	7433 ± 1	$0 - 500$	9.1E-20 $\pm$ 30%	
6C*0122+426	2.635	Lyα	1216	4420 ± 1	$600 - 1300$	1.8E-19 $\pm$ 10%	G
		CIII]	1909	3940 ± 2	$1100 - 2000$	6.1E-20 $\pm$ 10%	
6C*0128+394	0.929	MgII	2799	5389 ± 4	$400 - 1200$	6.3E-20 $\pm$ 20%	G
		[OII]	3727	7190 ± 2	$0 - 600$	6.8E-20 $\pm$ 5%	
6C*0132+330	1.710	CIII]	1909	5175 ± 1	$0 - 700$	8.0E-20 $\pm$ 10%	G
		CII]	2326	6304 ± 1	$0 - 700$	7.7E-20 $\pm$ 10%	
		[NeIV]	2424	6578 ± 1	$0 - 700$	5.0E-20 $\pm$ 10%	
6C*0133+486	1.029?	[OII]?	3727	7559 ± 1	$0 - 600$	1.8E-19 $\pm$ 15%	G

Source name	z	Line	λ_{rest} (Å)	λ_{obs} (Å)	FWHM (km s^{-1})	Flux (Wm^{-2})	Galaxy or Quasar
6C*0135+313	2.199	Lyα	1216	3900 ± 1	1500 − 2000	1.5E-17 ± 15%	G
		CIII]	1909	6058 ± 2	300 − 1000	3.1E-18 ± 15%	
6C*0136+388	1.108?	[OII]?	3727	7858 ± 3	800 − 1200	2.5E-16 ± 10%	G
6C*0139+344	1.637	[NeIV]	2424	6392 ± 3	400 − 800		G
		MgII	2799	7381 ± 2	700 − 1000		
		[NeV]	3426	9035 ± 2	200 − 400		
		[OII]	3727	9828 ± 1	500 − 800		
6C*0142+427	2.225	Lyα	1216	3921 ± 1	1100 − 1800	1.5E-18 ± 15%	G
		CIV	1549	5001 ± 1	900 − 1400	1.6E-19 ± 25%	
		HeII	1640	5284 ± 6	0 − 800	7.1E-20 ± 20%	
6C*0152+463	2.279	Lyα	1216	3987 ± 3	0 − 1200	3.8E-19 ± 30%	G
		HeII	1640	5393 ± 1	300 − 1100	1.2E-19 ± 25%	
6C*0154+450	1.295	CIV	1549	3554 ± 2	∼ 7000	1.6E-17 ± 20%	Q
		HeII	1640	3787 ± 2	∼ 4000	2.8E-18 ± 20%	
		CIII]	1909	4361 ± 15	∼ 5000	3.1E-18 ± 40%	
		MgII	2799	6422 ± 6	∼ 6000	2.3E-18 ± 35%	
		[OII]?	3727	8584 ± 4	< 3000	1.4E-18 ± 15%	
6C*0155+424	0.513	[OII]	3727	5639 ± 1	0 − 900	3.3E-19 ± 15%	G
		Hδ	4102	6205 ± 1	1000 − 1400	2.3E-19 ± 10%	
6C*0158+315	1.505	CII]	2326	5813 ± 3	0 − 600	5.9E-19 ± 15%	G
		[NeIV]	2424	6072 ± 3	0 − 600	6.6E-19 ± 10%	
		MgII	2799	7014 ± 1	200 − 850	1.4E-18 ± 10%	
6C*0201+499	1.981	Lyα†	1216	3625 ± 2	1200 − 2000	2.1E-19 ± 20%	G
		NV	1240	3692 ± 2	0 − 1000	2.5E-20 ± 20%	
		SiIV + OIV]	1402	4172 ± 9	1600 − 2100	1.0E-19 ± 15%	
		CIV	1549	4615 ± 3	1000 − 1600	4.5E-20 ± 40%	
		CII]	2326	6924 ± 8	1200 − 1500	8.1E-20 ± 20%	
		[NeIV]	2424	7242 ± 21	1600 − 2000	1.5E-19 ± 20%	
6C*0202+478	1.613?	CII]?!	2326	6066 ± 2	0 − 700	7.5E-19 ± 10%	G
		MgII?!	2799	7314 ± 3	0 − 700	5.8E-19 ± 20%	
6C*0208+344	1.920	Lyα	1216	3551 ± 2	1200 − 2000	4.1E-19 ± 10%	G
		CIV	1549	4524 ± 1	600 − 1400	1.0E-19 ± 10%	
		CII]	2326	6799 ± 1	400 − 900	9.9E-20 ± 10%	
6C*0209+476	1.141?	[OII]?	3727	7980 ± 1	200 − 600	1.9E-19 ± 5%	G

Table 2: Measurements obtained from the spectra of sources in the 6C* radio sample. The '?' denotes an uncertain line identification and the '!' denotes a feature which is possibly spurious. The † symbol means that the line is contaminated by a cosmic ray. For many of the uncertain lines in sources with known redshifts the line diagnostics are not presented because of the low signal-to-noise. For sources with redshifts based on uncertain lines, we present the emission line data for the emission lines which are likely to be real. Errors on the line fluxes represent the 1σ uncertainty expressed as a percentage of the best line-flux estimate, for the strongest lines these are dominated by roughly equal contributions from uncertainties in fixing the local continuum level, and from the absolute flux calibration (including plausible slit losses). Line widths were estimated from the FWHM of the best-fit Gaussian to each line, the lower value assumes the line-emitting region fills the slit, and the higher value assumes that it is broadened only by the seeing. The emission line fluxes for 6C*0106+397 are lower limits estimated by fitting a Gaussian from the maximum continuum level, as the spectrophotometric standard used to calibrate this observation was taken on a different night. For 6C*0118+486 we give emission line fluxes for the foreground galaxy (6C*0118+486b) in addition

(1)	(2)	(3)	(4)	(5)	(6)	(7)
Source	S_{151}	α_{151}	z	$\log_{10} L_{151}$	Line	$\log_{10} L_{\mathrm{line}}$
6C*0020+440	2.00	0.97	2.988	28.03	Lyα	36.37
6C*0024+356	1.09	0.69	2.161	27.33	Lyα	35.96
6C*0031+403	0.96	0.90	1.618	27.08	CIV	35.18
6C*0032+412	1.29	1.28	3.658	28.21	Lyα	36.35
6C*0041+469	1.53	0.61	2.145?	27.45	Lyα	35.55
6C*0050+419	1.00	1.24	1.748?	27.31	HeII?	34.16
6C*0052+471	1.31	0.88	1.935	27.38	Lyα	36.12
6C*0058+495	0.97	0.74	1.173	26.74	[OII]	35.92
6C*0106+397	0.96	0.52	2.284	27.25	CIV	34.87
6C*0112+372	1.03	0.42	2.535	27.36	Lyα	37.05
6C*0115+394	0.96	1.06	2.241	27.48	Lyα	37.15
6C*0118+486	0.98	1.47	2.350	27.70	Lyα	36.17
6C*0122+426	1.05	0.53	2.635	27.43	Lyα	35.97
6C*0128+394	1.94	0.50	0.929	26.75	[OII]	34.52
6C*0132+330	1.56	1.28	1.710	27.50	CIII]	35.19
6C*0133+486	1.89	1.22	1.029?	27.04	[OII]?	35.05
6C*0135+313	1.24	1.18	2.199	27.62	Lyα	37.71
6C*0136+388	0.99	0.68	1.108?	26.68	[OII]?	35.68
6C*0139+344	1.10	0.74	1.637	27.11	[OII]	-
6C*0140+326	1.00	0.62	4.410	27.94	Lyα	36.87
6C*0142+427	1.46	1.20	2.225	27.70	Lyα	36.72
6C*0152+463	1.29	0.79	2.279	27.49	Lyα	36.15
6C*0154+450	1.15	1.28	1.295	27.07	CIV	37.22
6C*0155+424	1.51	0.89	0.513	26.20	[OII]	34.66
6C*0158+315	1.51	0.75	1.505	27.16	MgII	36.31
6C*0201+499	1.14	0.74	1.981	27.30	Lyα	35.75
6C*0202+478	1.06	0.86	1.620?	27.13	CII]?	36.10
6C*0208+344	0.97	0.57	1.920	27.13	Lyα	36.01
6C*0209+476	1.14	0.69	1.141?	26.77	[OII]?	35.18

Table 3: Summary of key information on the 6C* sample. **Column 1:** Name of the 6C* source. **Column 2:** 151 MHz flux-density measurements in Jy from the 6C survey (Hales et al. 1993). **Column 3:** radio spectral index evaluated at rest-frame 151 MHz using the polynomial fit described in Blundell et al. (1998). **Column 4:** redshift, '?' signifies that this value is not yet an unequivocal redshift. **Column 5:** $\log_{10}$ of the rest-frame 151 MHz radio luminosity (measured in units of W Hz^{-1} sr^{-1}), calculated using the polynomial fit to the radio spectra. **Column 6:** Prominent emission line in the existing spectra, '?' signifies that the line identification is uncertain. **Column 7:** $\log_{10}$ of the line luminosity (measured in units of W), '−' means that the data are inadequate to obtain a line luminosity through the absence of a spectrophotometric standard.
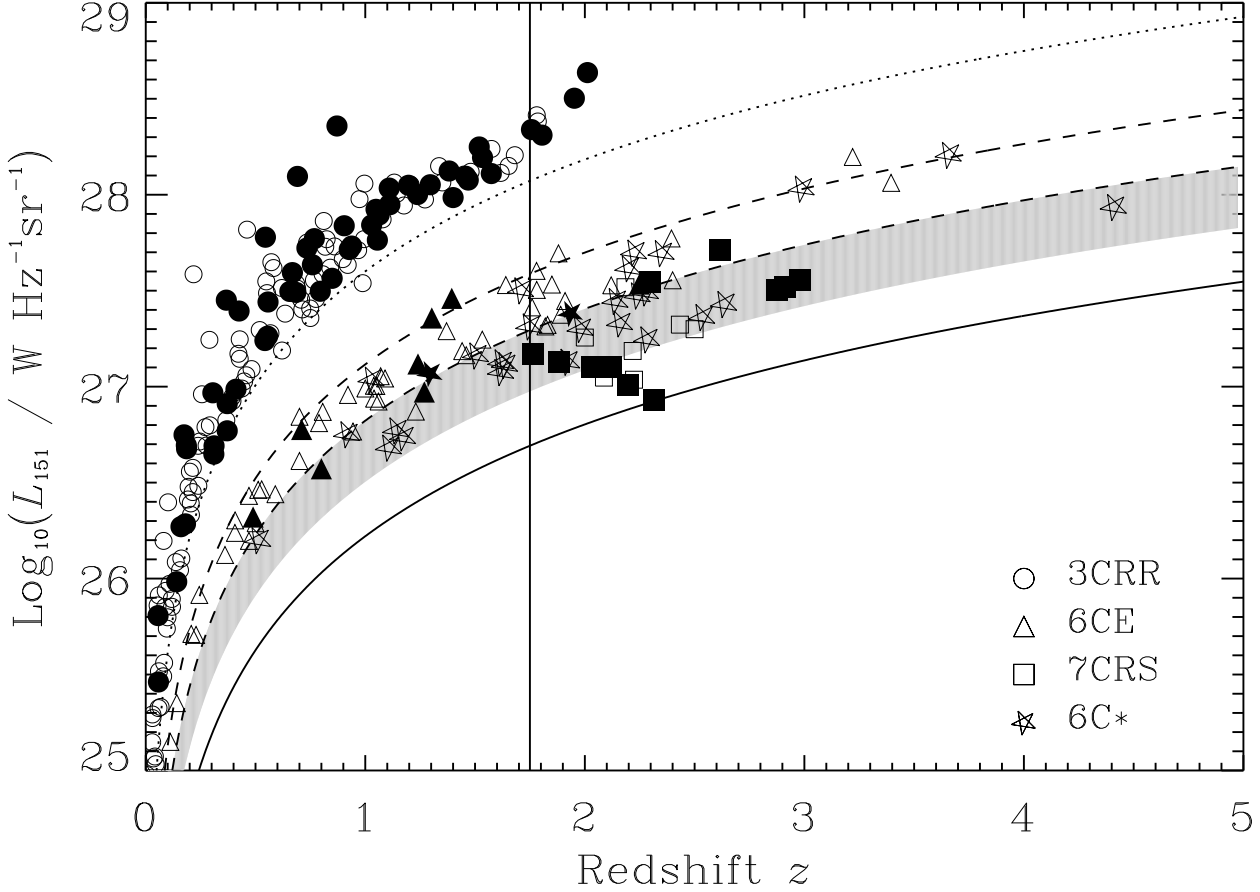
Figure 1: Rest-frame 151-MHz luminosity (L_{151}) versus redshift z plane for the 3CRR (circles), 6CE (triangles) and 6C* (stars) samples; the vertical line at $z = 1.75$ is the lower limit of the high-redshift sample considered in Sec. 6 and objects from regions I and II of the 7CRS sample with $z > 1.75$ are also plotted (squares). The open symbols are radio galaxies and the filled symbols are quasars. The rest-frame 151-MHz luminosity L_{151} has been calculated according to a polynomial fit to the radio spectrum [the relevant radio data can be found in Blundell et al. (1998) and Blundell et al. in prep]. The curved lines show the lower flux-density limit for the 3CRR sample (dotted line; Laing et al. 1983) and the 7CRS (solid line; Blundell et al. in prep; Willott et al. in prep). The dashed lines correspond to the limits for the 6CE sample (Rawlings et al. 2001) and the shaded region shows the 6C* flux-density limits (all assuming a low-frequency radio spectral index of 0.5). Note that the area between the 3CRR sources and 6CE sources contains no sources, this is the area which corresponds to the absence of a flux-density-limited sample between the 6CE ($S_{151} \leq 3.93$ Jy) and 3CRR ($S_{178} \geq 10.9$ Jy) samples. The reason why some of the sources lie very close to or below the flux-density limit of the samples represented by the curved lines is because the rest-frame 151-MHz spectral indices lie very close to or below the assumed spectral index of the curves of $\alpha = 0.5$.

4   NOTES ON INDIVIDUAL SOURCES

The radio maps referred to in this section can be found in Blundell et al. (1998) and the optical and $K-$band images referred to are presented in Jea01.

6C*0020+440 A blind spectrum was taken pointed at the mid-point of the two hotspots where there appears to be a faint K-band identification. Strong Lyα emission and probable CIVλ1549 Å emission point to a radio galaxy at $z = 2.988$. The $K-$band magnitude ($K = 18.9$ in a 5 arcsec aperture) is also consistent with the source being at this redshift.

6C*0024+356 We find a strong line at 3844 Å which we take to be Lyα at $z = 2.161$ and the presence of CII]λ2326 Å confirms this redshift.

6C*0031+403 Emission lines corresponding to CIVλ1549 Å and CIII]λ1909 Å give this a redshift of $z = 1.619$. There are also hints of CII]λ2326 Å and [NeIV]λ2424 Å in all of the 2-D spectra taken.

6C*0032+412 This is the second highest confirmed redshift object in the sample at $z = 3.658$, with strong Lyα emission and a faint but secure emission line corresponding to CIVλ1549 Å at this redshift. We also present a K-band spectrum of this source in

Fig. 3, which shows the presence of [OIII]λ4959 Å and [OIII]λ5007 Å at $z = 3.670$.

6C*0041+469 $K-$ and $I-$band imaging of this source reveals emission accurately aligned with the radio structure. Spectroscopic observations along this aligned component show tentative lines corresponding to Lyα, CIV and CIII] at $z = 2.140$, although further spectroscopy will be needed to confirm this. It is worth noting that at this redshift Hα is redshifted into the K-band window and the extended K-band emission may be dominated by line emission as has been found in other sources with extended optical/infrared emission aligned with the radio component (e.g. Egami et al. 1999). However, the K-band magnitude ($K = 19.2$ in an 8 arcsec aperture, Jea01) is consistent with this redshift using the $K - z$ diagram (e.g. Eales et al. 1997; Jea01).

6C*0050+419 The radio structure of this source is compact at 4.9 GHz with an angular size $\theta \lesssim 2$ arcsec. We pointed the telescope directly at the radio structure with a position angle of $41°$ which was chosen to align with the slightly extended radio structure in this direction. A total of 1 hour of optical spectroscopy with the Keck telescope reveals continuum at the position of the radio emission down to the limit of the spectral window of 4000Å, placing an upper limit on the redshift at $z \lesssim 3.4$ from the Lyman limit. We also identify four highly tentative lines, which could correspond to CIVλ1549Å, HeIIλ1640Å, CII]λ2326Å and [NeIV]λ2424Å at $z = 1.748$. Using the $K - z$ diagram, the K-band magnitude of this object ($K = 18.8$ in an 8 arcsec aperture) is also consistent with this redshift.

Subsequent deep I-band imaging with the Keck telescope reveals two faint components, both approximately 1.5 arcsec away from the centre of the radio emission, one to the south and one to the north-west (see Jea01), which for our chosen PA, the slit would have passed between. Whether this emission is associated with the radio source has yet to be confirmed. Further spectroscopy on the WHT in February 2000 with a PA aligned to encompass these two components failed to yield any bright emission lines or detectable continuum (note that Lyα at $z = 1.748$ would fall in a region of very low signal-to-noise in our spectrum). In summary our observations are consistent with a faint K-band ID at the position of the southern $I-$band object (object 'a' in Jea01) and with an additional $I-$band component to the north-west.

There is also the possibility that the source of the radio emission may be from an object ≈ 7 arcsec to the south-west of the centre of the bright radio emission (object 'b' in Jea01). This is roughly in the direction of the slightly extended radio structure, and is co-spatial with a faint radio component in our 8.4 GHz map. Our existing spectroscopy marginally passes through this object and there are hints of the same emission-lines as those detected towards the centre of the bright radio emission, therefore this is a plausible candidate for the ID of the radio source and suggests that there is an aligned component in the optical/near-IR bands.

6C*0052+471 Strong and broad CIVλ1549 Å and CIII]λ1909 Å emission lines confirm this is a quasar at $z = 1.935$. There is also evidence for weaker Lyα emission and a decreasing continuum blueward of the CIV emission. This may be due to light reddening of the quasar by dust (e.g. Willott, Rawlings & Jarvis 2000a).

6C*0058+495 Strong [OII]λ3727 Å emission along with weaker lines corresponding to CIII]λ1909 Å , CII]λ2326 Å and MgIIλ2799 Å identify this as a radio galaxy at $z = 1.173$. There is also a line which corresponds to [SII]λ4072 Å which is not usually as strong as the line seen in our spectrum at the corresponding wavelength for this redshift. This emission line does not have any contamination from cosmic rays and is apparent in the 2-D spectra. Comparison of the [OII] and [SII] line fluxes for radio galaxies using the ratios of McCarthy (1993) gives a [OII] to [SII] ratio of 25:1, and the ratio in our spectrum is ≈ 5:2. Thus, if real, this feature is unusually strong for a radio galaxy spectrum.

6C*0106+397 A blind spectrum was taken pointed at the mid-point of the hotspots with LRIS on the Keck telescope and three definite emission lines confirm this as a radio galaxy at $z = 2.284$. Emission-line fluxes are estimated using a spectrophotometric standard taken on a different night, so the emission-line luminosities may be unreliable. The limited wavelength coverage of the LRIS spectrum means that we have no data on the Lyα line. There is also a bright object ($K = 17.8$ in an 8 arcsec aperture) ≈ 5 arcsec to the south-east of the radio galaxy ID which was aligned with our slit. A strong emission line at 6084 Å which we associate with [OII]λ3727 Å, and a blue continuum at the position of this object, lead us to conclude that it is a foreground galaxy at $z = 0.632$ and is not associated with the radio emission.

6C*0112+372 Blind spectroscopy at the Lick telescope, pointed at the bright radio component in our 4.9 GHz map, shows a bright emission line at the same wavelength as a single line identification from spectra obtained at the WHT in 1991 which we thought to be Lyα at $z = 2.535$. The detection of another line at 5476 Å from our Lick spectrum corresponding to CIVλ1549 Å confirms this as a radio galaxy at $z = 2.535$.

6C*0115+394 The redshift of this object is based on five emission lines.

6C*0118+486 This source has strong Lyα with corresponding CIVλ1549 Å and CII]λ2326 Å emission at $z = 2.350$. We also identify three emission lines, marked (a), (b) and (c) in Fig. 2, which correspond to [OII]λ3727 Å , H$\beta\lambda$4861 Å and possibly [OIII]λ5007 Å at $z = 0.529$. These lines suggest that there may be a foreground galaxy along or near the line of sight of this source. We defer discussion of this to Jea01. There also

appears to be absorption in the Lyα profile most likely due to associated H I absorption (see Sec. 6.2).

6C*0122+426 A Lyα line at $z = 2.635$ and a definite line corresponding to CIII]λ2326 Å place this source at $z = 2.635$. Observations on the Lick telescope confirm the other lines at this redshift.

6C*0128+394 Spectra from both 1995 and 1998 show a clear emission line at 7190 Å which we associate with [OII]λ3727 Å at $z = 0.929$. Further faint lines corresponding to MgIIλ2799 and [NeIV]λ2424 confirm this redshift.

6C*0132+330 The redshift of this source is based on three definite emission lines and a possible fourth; Lyα is too far blueward of our spectrum to detect.

6C*0133+486 Our K-band image shows two objects aligned with the radio emission. The source of the radio emission is therefore ambiguous. Our tentative identification of [OII]λ3727 Å at $z = 1.029$ at the position of the brighter optical ID is mildly supported by very weak MgIIλ2799 Å and CII]λ2326 Å at this redshift. This object has $K = 18.7$ (5 arcsec aperture), which, using the $K-z$ diagram (Eales et al. 1997; Jea01) is consistent with this redshift (although slightly fainter than mean relation). Further spectroscopic observations are needed to confirm this redshift.

6C*0135+313 $z = 2.199$ radio galaxy with strong Lyα and CIII]λ1909 Å. The Lyα emission is split into two peaks at 3893 Å and 3909 Å with a trough between them. This is possibly due to H I absorption associated with the host galaxy. The projected linear size of the radio emission is small ($D \approx 15\,$kpc), consistent with the results of van Ojik et al. (1997) in which small ($< 50\,$kpc) radio sources are more likely to exhibit associated H I absorption. The CIVλ1549 Å and HeIIλ1640 Å lines have FWHM < 10 Å and could be spurious.

6C*0136+388 The $K-$band identification for this source is spatially coincident with the brightest feature in the 4.9 GHz map, which also has a spectral index ~ 0 and is most likely the core. Optical spectra taken on the WHT in 1995 are inconclusive regarding the redshift of this source, mainly due to the poor seeing, although there is faint continuum visible down to at least ~ 4000 Å. Our more recent observation in Dec 1998 only provided spectra from the red-arm of ISIS due to a technical fault in the blue-arm observation. There is a strong emission line at 7858 Å in these spectra, and along with the evidence of continuum into the blue from the previous observations, we take this line to be [OII]λ3727 Å at $z = 1.108$. The K-band magnitude of ~ 17.3 (8 arcsec aperture) also suggests a redshift around this value.

6C*0139+344 The spectroscopic observations of this source highlight the problems associated with assigning redshifts on the basis of a single line. Spectroscopy for this source was initially attempted on the WHT in 1992 and again in 1995. The spectrum from the 1995 run showed a bright emission line at 7381 Å. This

was initially thought to be Lyα at $z = 5.07$ as there was no obvious continuum or emission lines blueward of this line. However, its proximity to a $z = 0.37$ foreground galaxy (~ 2.5 arcsec to the north) and the lack of a second emission line prevented conclusive proof. We then obtained an optical spectrum, dispersed at a longer wavelength to search for CIVλ1549 Å at $\lambda = 9402$ Å on the Keck-II telescope. However, the presence of a bright emission line at 9828 Å meant that the lines are now identified with MgIIλ2799 Å and [OII]λ3727 Å at $z = 1.637$. The lack of a spectrophotometric standard for the set-up used to take this spectrum makes it impossible to flux calibrate the spectrum. Thus, although we present a spectrum in Fig. 2, the flux-density scale can only be used to estimate relative fluxes since no absolute line fluxes are available at present.

6C*0140+326 The highest redshift source in the sample at $z = 4.41$; the radio emission is likely to be gravitationally amplified by a factor $\lesssim 2.0$ by a $z = 0.927$ galaxy ~ 1.6 arcsec from the eastern radio lobe (see Rawlings et al. 1996). Deeper Keck spectroscopy and imaging of this object can be found in De Breuck (2000c) and van Breugel et al. (1998).

6C*0142+427 Strong Lyα and very weak CIVλ1549 Å co-spatial with the central core component in the radio map confirm this as a radio galaxy at $z = 2.225$. There is also some Lyα emission ~ 5 arcsec to the south-east, which is probably associated with the lobe.

6C*0152+463 The presence of strong Lyα and HeII in our spectrum confirm this as a radio galaxy at $z = 2.279$.

6C*0154+450 Broad CIVλ1549 Å and MgIIλ2799 Å confirm this source as a quasar at $z = 1.295$.

6C*0155+424 Three bright objects lie close to the radio source in the $R-$ and $K-$band images. The object closest to the centre of the radio emission is a galaxy at $z = 0.513$. This is separated from another object to the north-west by $\lesssim 2$ arcsec. The seeing for our spectroscopic observations was not sufficient to clearly resolve these two objects. We do not have a spectrum for the third spatially-resolved object ~ 4 arcsec to the south-east of the central object. These objects will be discussed in more detail in Jea01.

6C*0158+315 It was unclear from our radio map whether this source was a discrete object or a hotspot of a larger source. In our R- and K-band imaging we find an object co-spatial with the peak of the radio emission which we now take to be the radio galaxy. Definite lines corresponding to MgIIλ2799 Å, [NeIV]λ2424 Å and CII]λ2326 Å confirm this source at $z = 1.505$. The NVSS radio map shows that the radio component associated with the optical ID could conceivably be the core of a large ($\theta \sim 14$ arcmin) triple source, if this is the case then this source should be excluded from the final sample, but if this were true the

linear size of the source would be huge ($\approx 7\,\mathrm{Mpc}$ for $\Omega_{\mathrm{M}} = 1$, $\Omega_{\Lambda} = 0$).

6C*0201+499 The redshift of this source is based on five emission lines. The single exposure including the Lyα emission line has a cosmic ray in close proximity which may contribute to the flux measurement in Table 2.

6C*0202+478 The near-infrared ID for this source is in very close proximity to two bright stars, consequently the 1-D extraction of the spectrum does not show the emission lines very well. However, inspection of the 2-D spectrum shows a definite emission line at 7314Å, this would correspond to MgII at $z = 1.613$. There are also faint lines corresponding to [NeIV]λ2424, CII]λ2326 Å, CIII]λ1909 Å and CIVλ1549 Å at this redshift, which, if on their own would be inconclusive but collectively suggest that this redshift is correct.

6C*0208+344 Three definite emission lines place this source at $z = 1.920$. The Lyα emission also appears to have associated HI absorption (see Sec. 6.2).

6C*0209+276 This source has an identification in K-band which is coincident with the peak of the radio emission. Spectroscopy reveals an emission line which we take to be [OII]λ3727 Å at $z = 1.141$, there is also possibly an emission line corresponding to MgIIλ2799 Å at this redshift. A slight worry was that the emission line appeared to be offset from the expected target row on the ISIS detector (and there were no field objects along the slit to bootstrap the astrometry). Further imaging and spectroscopy may be needed to confirm whether this line emission is associated with the radio source and also if it is definitely [OII]. However, the K-band magnitude ($K = 18.1$ in an 8 arcsec aperture) is consistent with this redshift.

Figure 3: The UKIRT $K-$band spectrum of 6C 0032+412. This spectrum was obtained with the CGS4 spectrometer on UKIRT in Dec 1993 with the 75 lines mm^{-1} grating, and employed the standard nodding pattern (e.g. Eales & Rawlings 1993) with a nod of 34 arcsec (11 detector rows); the 20s exposures were arranged in sets of four shifted by 0, 0.5, 1, and 1.5 pixels in wavelength – this provided Nyquist wavelength sampling and ensured that a given wavelength was sampled by two pixels; the total exposure time for the final 126-pixel spectrum is $\approx 1800\,\mathrm{seconds}$, taken with a slit width of 3.1 arcsec. These data were extracted from a single detector row (3.1 arcsec) and have not been smoothed. The redshift of the [OIII]5007 line is $z = 3.670 \pm 0.005$, other parameters of the [OIII]5007 line are: measured FWHM = 1350 km s^{-1} (deconvolved value ≈ 1000 km s^{-1}); and line flux within ± 20 per cent of 1.6×10^{-18} W m^{-2}.

5 6C* - WHAT ARE WE MISSING FROM A FILTERED SAMPLE?

With the 6C* sample we are now able to compare the properties of this filtered sample with the recently completed 6CE sample (Rawlings et al. 2001) and 7CRS (Blundell et al. in prep; Willott et al. in prep). The number of sources in the 6C catalogue within the 6C* flux-density limits and over the same sky-area before filtering was 279, for which we would expect the median redshift to be the similar to that of 6CE and 7CRS, i.e. ~ 1.1 (Rawlings et al. 2001; Willott et al. in prep.). The median redshift of the 29 6C* sources is $z \approx 1.9$. As 6CE and 7CRS span flux-densities either side of the flux-density range of 6C*, we can conclude that the filtering criteria were effective in biasing the sample to objects at high redshift. However, the main problem in dealing with and interpreting a filtered sample such as 6C* is that it is difficult to assess the properties of the population which are omitted from the sample. In this section we use the most recently derived radio luminos-
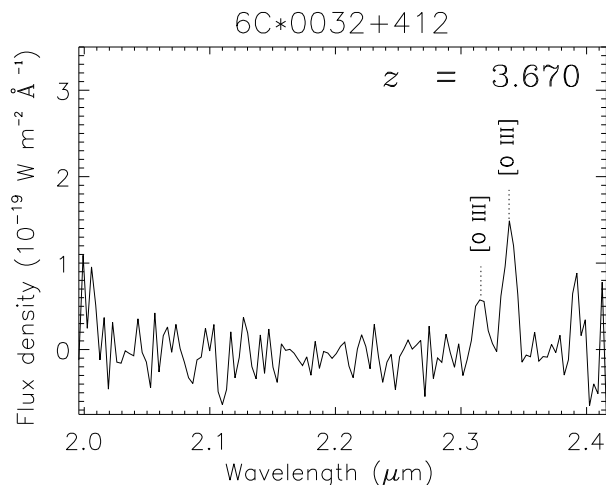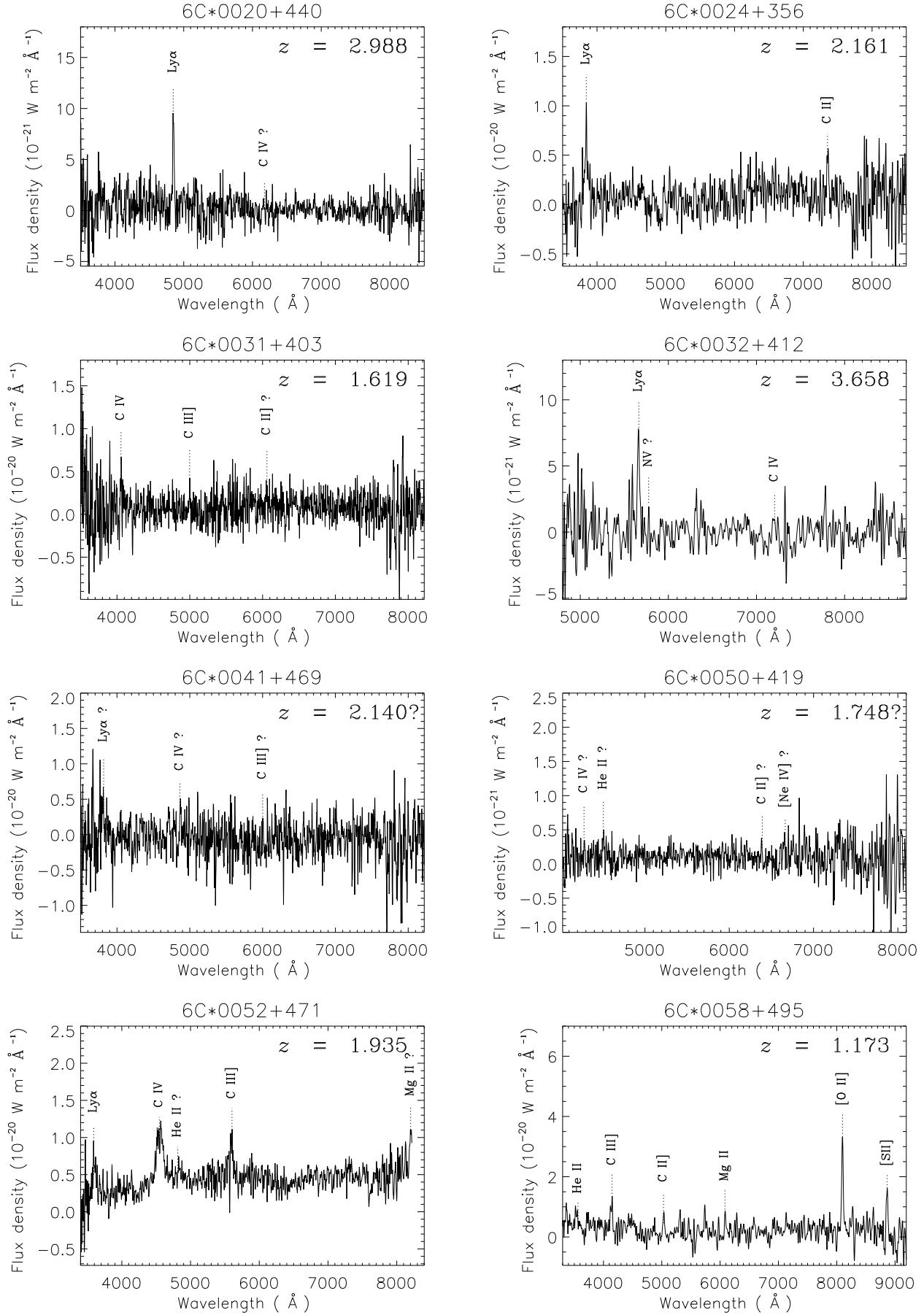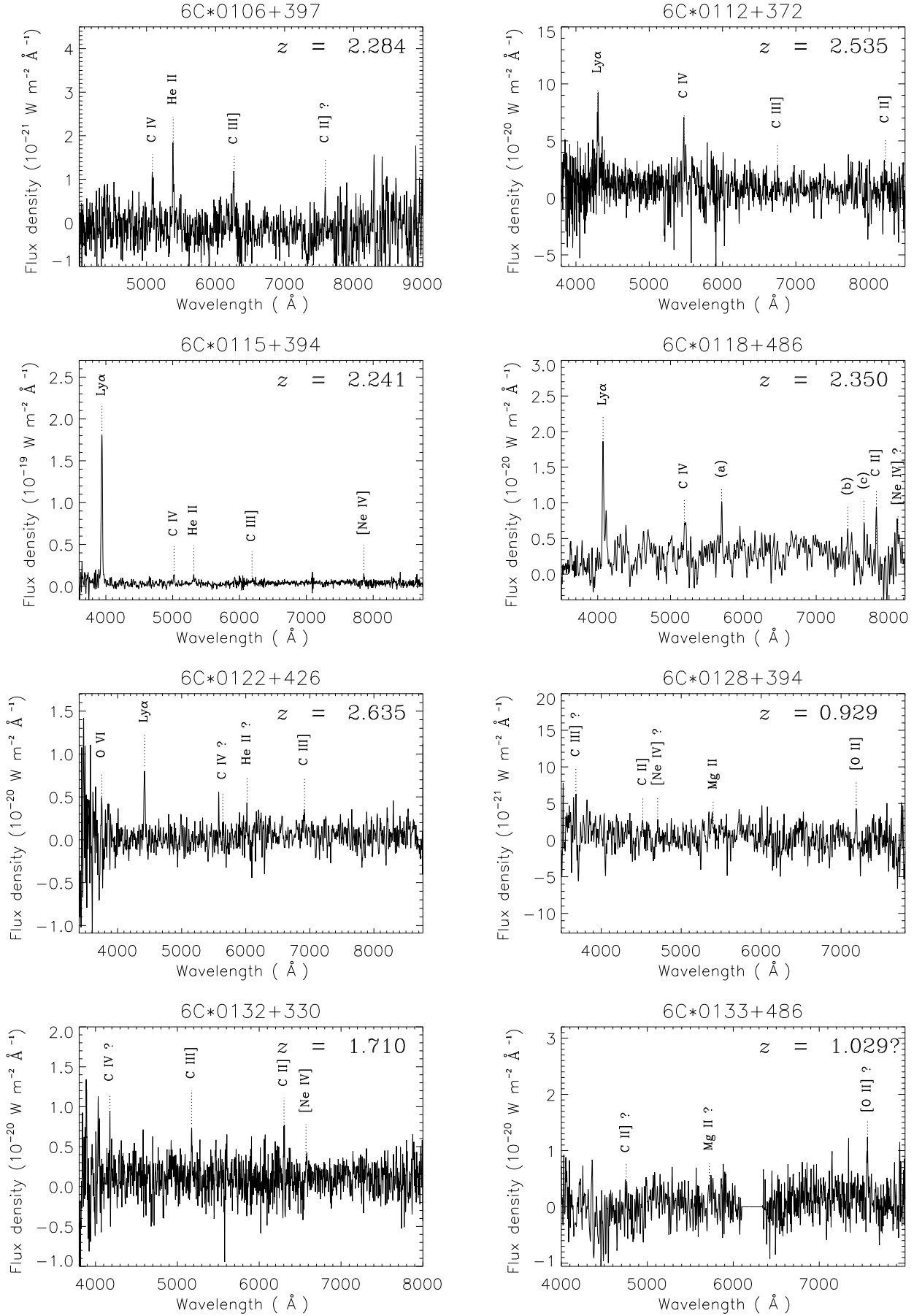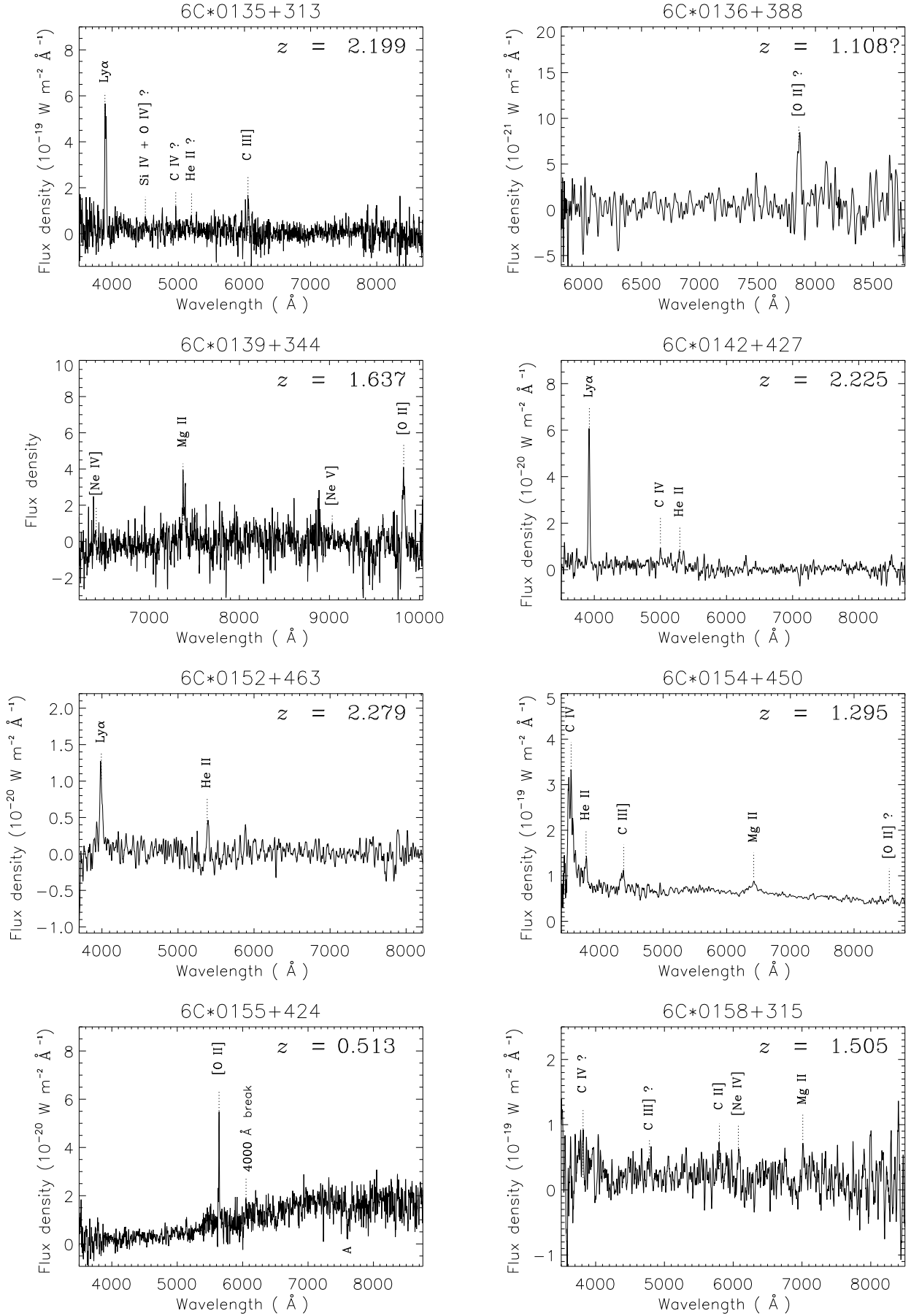
ity function for low-frequency selected radio samples of Willott et al. (2001a) to estimate the fraction of sources excluded from 6C* over the redshift space probed. This is different to the analysis of Jarvis et al. (2001a) which estimated the fraction of only the most luminous population of radio sources which were excluded from 6C*. Here we discuss the effects of the selection criteria across the whole radio luminosity range.

Fig. 4 shows the redshift distribution of the 6C* sample on a logarithmic axis. One can immediately see that this distribution is significantly different from the predicted distribution from the three models for the RLF of Willott et al. (2001a), with the distribution skewed towards objects at $z \gtrsim 2.0$, as expected. Indeed, employing the selection criteria has reduced the number of $z < 1.5$ sources by $\approx 90\%$, whereas in the redshift range $1.5 \lesssim z \lesssim 3.0$ the fraction excluded varies from $\sim 70\%$ to $\sim 30\%$. However, this sample was initially designed to find objects at $z > 4$, and with the discovery of the $z = 4.41$ radio galaxy 6C*0140+326, (and 6C*0032+412 at $z = 3.658$) the sample has proven a
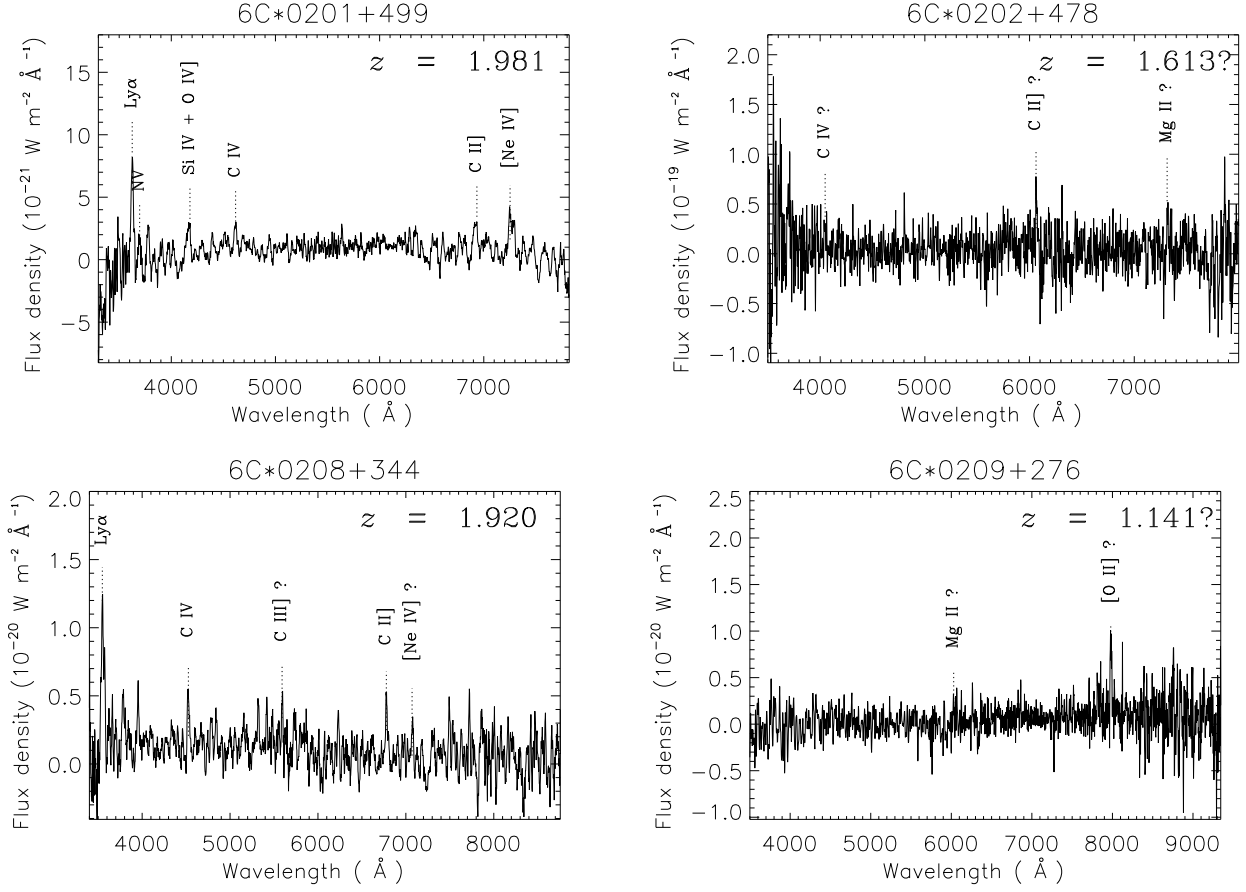
6C*0020+440

z = 2.988

Lyα

C IV ?

6C*0024+356

z = 2.161

Lyα

C II

6C*0031+403

z = 1.619

C IV

C III]

C II] ?

6C*0032+412

z = 3.658

Lyα

NV ?

C IV

6C*0041+469

z = 2.140?

Lyα ?

C IV ?

C III] ?

6C*0050+419

z = 1.748?

C IV ?

He II ?

C II] ?

[Ne IV] ?

6C*0052+471

z = 1.935

Lyα

C IV

He II ?

C III]

Mg II ?

6C*0058+495

z = 1.173

He II

C III]

C II]

Mg II

[O II]

[SII]

6C*0106+397 $z = 2.284$

6C*0112+372 $z = 2.535$

6C*0115+394 $z = 2.241$

6C*0118+486 $z = 2.350$

6C*0122+426 $z = 2.635$

6C*0128+394 $z = 0.929$

6C*0132+330 $z = 1.710$

6C*0133+486 $z = 1.029?$

6C*0135+313 $z = 2.199$

6C*0136+388 $z = 1.108?$

6C*0139+344 $z = 1.637$

6C*0142+427 $z = 2.225$

6C*0152+463 $z = 2.279$

6C*0154+450 $z = 1.295$

6C*0155+424 $z = 0.513$

6C*0158+315 $z = 1.505$

Figure 2: Spectra of the 6C* sources obtained with the various telescopes and instruments mentioned in Sec. 3, with the emission line identifications. Possible emission lines are marked with a '?'. The emission lines which do not appear as significant detections in the 1-D spectra, and which are not marked with '?', are significant in the 2-D spectra. The gap in the spectrum of 6C*0133+486 is a result of combining blue- and red-arm spectra where the short wavelength end of the red spectrum suffered technical problems. The flux density scale for the spectrum of 6C*0139+344 is measured in W m^{-2} Å^{-1} with arbitrary normalisation, due to the lack of a spectrophotometric standard.

success. The expected number of sources at these high redshifts in the 6C* sky area in the absence of the selection criteria is only $\sim 1 - 2$, even if there is no redshift cut-off above $z \sim 2.5$ in the steep-spectrum population (c.f. Dunlop & Peacock 1990; Willott et al. 2001a). Thus, the discovery of these two high-redshift objects from a sample of just 29 radio sources, relates both to a very high efficiency for the detection of $z \gtrsim 3.5$ objects in the selection techniques used, and to the absence of an abrupt cut-off in the intrinsic co-moving space density (Jarvis et al. 2001a). This has already led to the re-assessment of the evolution in the co-moving space density of the most luminous steep-spectrum radio sources (Jarvis et al. 2001a) resulting in a best-fit evolutionary scenario in which the space density of these sources remains roughly constant out to at least the limit of the 6C* data at $z = 4.41$.

The effects of the selection criteria on the luminosity distribution are also illustrated in Fig. 4. The skewness of the distribution to high luminosity illustrates the effect of the biases inherent in the sample. Our purpose, to find radio galaxies at high redshift, necessarily skews the luminosity distribution to the bright end if the filtering criteria are effective. Thus the skewness is accentuated in the filtered sample compared to complete samples.

We have shown that the filtering criteria of 6C* are efficient in finding objects at high redshift, however it is extremely difficult to decouple the two mechanisms which are causing this bias. The steep-spectral index selection technique is widely used in targeting high-redshift objects, but the effectiveness of this has yet to be properly quantified (De Breuck et al. 2000a). The angular size constraint has been less widely used and until the physics of radio sources and the cosmic evolution of radio source environments are fully understood, the effect this may have on radio samples will probably be similarly hard to quantify. We do know, however, that these two selection criteria work against finding low-redshift, low-luminosity sources in flux-density-limited samples, and thus, for searches for high-redshift sources they are proven to be extremely effective.

6 LINKING THE RADIO AND OPTICAL PROPERTIES OF LUMINOUS HIGH-REDSHIFT RADIO SOURCES

There has been extensive work in recent years on linking the optical properties of radio sources with their radio properties. A recent review can be found in Willott et al. (1999), who used a combined sample comprising 3CRR and 7CRS radio sources to decouple trends with redshift from trends in luminosity. They found a strong correlation between the narrow emission-line luminosity and the rest-frame 151-MHz radio luminosity, but only weak correlations between the luminosity of the

narrow emission lines and projected linear size D or rest-frame spectral index. Best, Röttgering & Longair (2000) from a sample of 3CR radio galaxies at $z \sim 1$ found evidence that the radio sources with small linear sizes ($D \sim 100$ kpc) have lower ionisation states, higher [OII] emission-line fluxes and broader [OII] line widths than the larger sources. Using a sample of 18 objects selected to have good signal-to-noise spectra and UV/optical emission with large spatial extents, van Ojik et al. (1997) found a correlation between the radio source size and the extent of the Lyα emission-line gas in high-redshift ($z > 2.1$) radio galaxies with $10 \lesssim D \lesssim 100$ kpc. They also found a high fraction ($\sim 90\%$) of HI absorbed Lyα profiles in those with $D \lesssim 50$ kpc.

With the 6C* sample in conjunction with the 3CRR and 6CE samples and the 7CRS, we are now able to extend these investigations to higher redshifts. We have chosen to confine our attention to radio galaxies in the complete samples. According to simple unified schemes (e.g. Willott et al. 2000b) we are therefore focusing on the sub-set of sources with jet-axes within $\sim 53°$ of the plane-of-the-sky which has the obvious advantage that D should be within a factor $0.6 - 1.0$ of the true linear size[†].

Correlations between the logarithms of various radio and optical properties are presented: 'best-fit' lines are calculated using an algorithm which minimises the sum of the square of the perpendicular distances from the data points to a line with adjustable slope and intercept (see discussion in Jaynes 1991).

6.1 $L_{Ly\alpha}$ versus radio luminosity

In Fig. 5 we plot the Lyα emission-line luminosity $L_{Ly\alpha}$ against the 151-MHz radio luminosity L_{151} for a sample of 35 radio galaxies with $z > 1.75$, derived from the 3CRR, 6CE and 7CRS samples along with the 6C* sample.[‡]

[†] Note however, from Fig. 1 that the quasar fraction at $z > 1.75$ in our combined dataset is somewhat lower than the 0.4 seen at similar radio luminosities at lower redshift (Willott et al. 2000b). Considering only flux-density-limited samples Rawlings et al. (2001) have recently argued that this may be a statistical fluke, although an epoch dependent increase in reddening (e.g. Willott, Rawlings & Jarvis 2000a) may play a rôle. We note for 6C* that the filtering criteria both bias in favour of quasars (objects closer to the line-of-sight will have a smaller angular size for a given true linear size) and against them (objects closer to the line-of-sight may have significant Doppler-boosted components which flatten their spectral index), so it is difficult to interpret the quasar fraction of this sample (see Jarvis 2000).

[‡] As illustrated in Fig. 1 there are 38 radio galaxies in our dataset at $z > 1.75$. In this analysis we include only those with a measured Lyα flux. This excludes the 6C* radio galaxy 6C*0106+397 (for which we do not have spectra around the Lyα line) and the 7CRS radio galaxies 5C6.242 (7C0218+3103) and 5C7.208 (7C0820+2506). The two 7CRS exclusions are because these galaxies have no emission lines in their optical spectra and
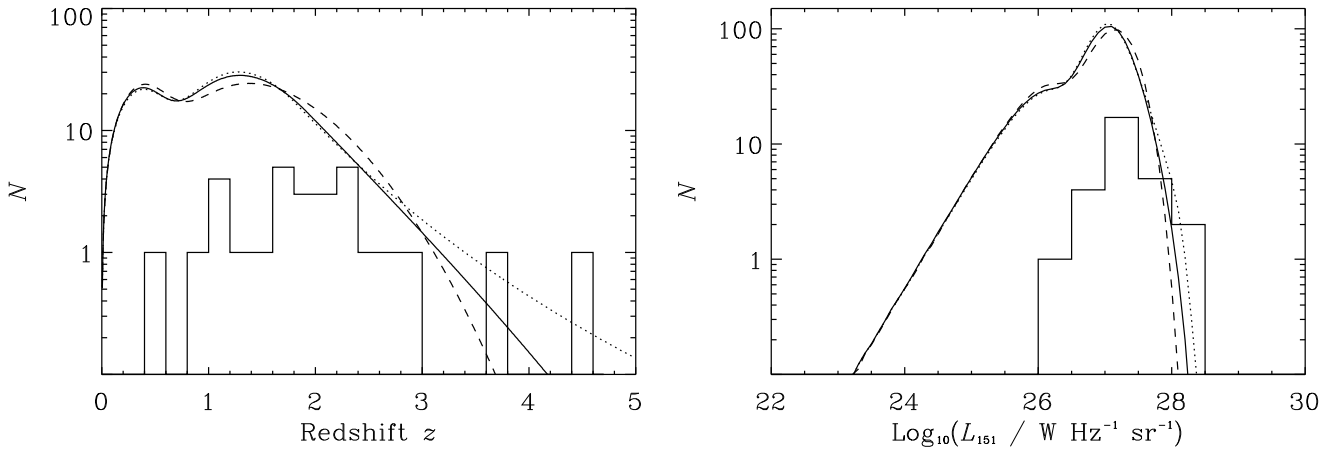
Figure 4: (left) Histogram of the redshift distribution $N(z)$ of the 6C* sample; the bin width is $\Delta z = 0.2$. (right) Histogram of the 151 MHz rest-frame luminosity distribution $N(\log_{10} L_{151})$ of the 6C* sample; the bin width is $\Delta(\log_{10} L_{151}) = 0.5$. Also shown are the source count predictions for the flux-density range of 6C* ($0.96\,\mathrm{Jy} \leq S_{151} \leq 2.00\,\mathrm{Jy}$) from the three best-fit RLF models from Willott et al. (2001a) with no filtering applied. The dashed line corresponds to their model A (a cut-off at high redshift similar to the decline at low-redshift); the dotted line to model B (constant co-moving space density above a peak redshift); and the solid line to model C (a Gaussian decline at high redshift decoupled from the low-redshift evolution).

It is apparent that a strong correlation exists between the $L_{\mathrm{Ly}\alpha}$ and L_{151} for the radio galaxies present in this subsample. The strength of this correlation is quantified using the Spearman partial rank correlation coefficient (e.g. Macklin 1982) and the results are presented in Table 4; note that the use of a combined 3CRR, 6CE, 7CRS and 6C* dataset severely weakens the strong correlations between L_{151} and z in a single flux-density-limited sample (as illustrated in Fig. 1).

The best-fit line has a slope of 1.49 ± 0.25 which is steeper than the power-law index found by Willott et al. (1999) for the [OII] luminosity versus L_{151} for sources from the 3CRR and 7CRS [which using the same algorithm is 1.00 ± 0.04, for the analysis which includes 6CE (see Willott 2000)].

Any 'least-squares' algorithm is sensitive to anomalous outliers, so we have investigated this by excluding 5C7.271 (7C0826+2504), which has $\log_{10} L_{\mathrm{Ly}\alpha} = 34.73$ and is thus more than 0.5 dex lower than any of the other sources, and is below the radio luminosity at which the quasar fraction of radio sources is no longer independent of luminosity and/or redshift (Willott et al. 2000b). We also exclude 6C*0135+313 which appears to be anomalously bright in Lyα. Excluding these sources we find that the correlation becomes 1.33 ± 0.21. Thus, although we are spanning only 1.5 dex in radio luminos-

ity we find a tight correlation between $L_{\mathrm{Ly}\alpha}$ and L_{151} (with a Gaussian 1σ spread of 0.12 perpendicular to the best-fit line) which is marginally steeper than that found by Willott et al. (1999) for the correlation between $L_{\mathrm{[OII]}}$ and L_{151}.

If we also include the high-redshift sample of De Breuck et al. (2000b), which includes high-redshift sources selected on account of their steep radio spectral indices (which is similar, but not identical to the spectral index criterion of 6C*), then we find that the slope of this correlation flattens to 0.87 ± 0.10 [§]. At $z > 1.75$ Lyα lies within the observable optical window, and is typically detected at many times the detection limit, so there should not be a large number of $z > 1.75$ objects missing in a systematic way from the De Breuck et al. compilation. Because of the restricted size of our 3CRR/6CE/7CRS/6C* dataset, and the consequences of differing filtering criteria in larger compilations, it is difficult at this stage to conclude much beyond a rough proportionality between Lyα and L_{151} for luminous radio sources.

The results presented here further strengthen the evidence for a link close to a proportionality between L_{151} and narrow-line luminosity (e.g. Willott et al. 1999), and suggest its roughly redshift-independent

---

hence only photometric redshifts (Willott, Rawlings & Blundell 2001b): their exclusion does not affect any of the results as even if they truly lie at $z > 1.75$ their line strengths will be weak, placing them at the bottom left of the plots in Fig. 5 in line with the correlation discussed in Sec. 6.1.

[§] The radio luminosities calculated by De Breuck et al. were for a rest-frame frequency of 325 MHz so we have estimated L_{151} assuming a spectral index of $\alpha = 1.0$. This flatter spectral index should thus compensate for any intrinsic spectral curvature in these objects between the relatively high frequency α measured and that at rest-frame 151 MHz.

Correlated variables: A, B	r_{AB}	P_r	$r_{AB,C}$	σ
$L_{151}, L_{Ly\alpha}$	0.619	$< 0.1\%$	0.679	4.603
L_{151}, z	0.242	16%	0.421	2.497
$L_{Ly\alpha}, z$	-0.138	43%	-0.378	2.212

Table 4: Spearman rank correlation analysis of the correlations present between L_{151}, $L_{Ly\alpha}$ and z for the 35 objects in our subsample at $z > 1.75$. r_{AB} is the Spearman rank coefficient between the parameters A and B, P_r is the two-tailed probability that a given value of r is predicted by chance, given the null hypothesis that A and B are unrelated and σ is equivalent to the deviation from a unit variance normal distribution if there is no correlation present. $r_{AB,C}$ is the partial rank coefficient (e.g. Macklin 1982), this assesses the statistical significance of correlations between the variables A and B in the presence of the third variable, C. The significance of the partial rank correlation is equivalent to the deviation from a unit variance normal distribution if there is no correlation present.

form is maintained to $z \sim 4.5$. The physical origin of this link is somewhat controversial: following Rawlings & Saunders (1991), Willott et al. (1999) favour a close tie between the luminosity of the quasar nucleus and the bulk power carried by the radio jets; however, other authors (e.g. Bicknell, Dopita & O'Dea 1997; Koekemoer & Bicknell 1998) favour models in which the line-emitting gas is photoionised by shocks driven by the radio emitting components.

6.2 Radio source size and the emission line luminosities

Best et al. (2000) find that the theoretical predictions of shock ionisation models agree with the emission line ratios of CIII]1909/CII2326 and [NeIII]3869/[NeV]3426 for smaller sources, whereas the emission-line ratios in larger sources are consistent with the ionising photons being emitted directly from active nuclei.

Using the 7CRS, 6CE and 6C* samples we investigate this result for sources at $z > 1.75$. The angular sizes and projected linear sizes of these sources are summarised in Blundell et al. (1998) and Blundell et al. (in prep). At these redshifts the [NeIII] 3869 and [NeV] 3426 emission lines are redshifted out of the optical window, thus we are forced to use only the CIII] 1909 and CII 2326 emission lines. Although the majority of spectra for these sources span the waveband which would capture both the CIII] and CII] lines, the depth and signal-to-noise ratio of the observations are insufficient to calculate ratios for individual sources. Therefore, we chose to split the data into two broad bins in projected linear size. The median projected linear size
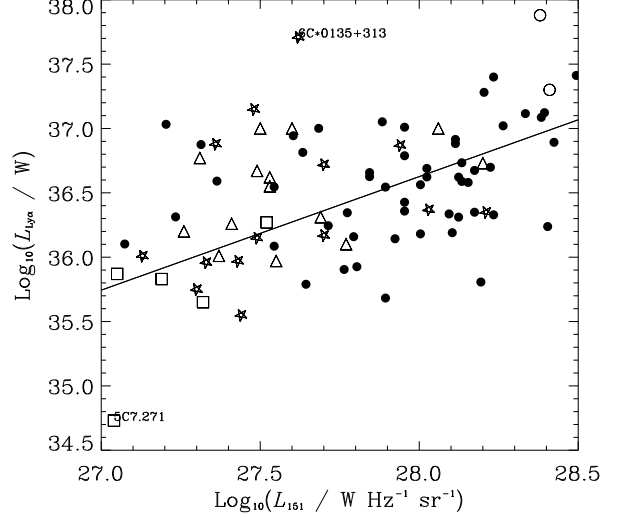

Figure 5: Lyα emission line luminosity, $L_{Ly\alpha}$, against rest-frame 151 MHz radio luminosity, L_{151} for radio galaxies at $z > 1.75$ from the 3CRR (circles), 7CRS (squares), 6CE (triangles) and 6C* (stars) radio samples. The filled circles are the high-redshift steep-spectrum sources from de Breuck et al. (2000b). The solid line shows the best-fit to all of the points shown.

of the 28 sources[¶] used in this analysis is ≈ 70 kpc, thus we use this as the division between two bins. We then combine the spectra in each bin to form a composite radio galaxy spectrum for sources in the two bins, following the same method of combination as Rawlings et al. (2001). These composites are shown in Fig. 6. It is apparent that there is a difference between the two, with the smaller sources having a CIII] 1909/CII] 2326 ratio of ~ 0.5 and the larger sources having CIII] 1909/CII] 2326 ~ 1.3. It is also apparent that in the composite of the larger sources, the CIV and particularly the HeII emission lines are much stronger than in the small source composite. This is in quantitative agreement with the findings of the Best et al. study of 3C sources at $z \sim 1$ (which as shown in Fig. 1, are of comparable L_{151}). We also split the data into two radio luminosity bins to investigate any dependence of the line ratios on the radio luminosity of the source.

[¶] Of the 38 sources in our dataset this sub-sample excludes objects lacking spectra available in an electronic format; namely both 3CRR sources (3C239 and 3C294) and 6CE0902+3419, 6CE1141+3525, 6CE1204+3708 and 6CE1232+3942 from the 6CE sample. 6C*0041+469 and 6C*0106+397 from 6C* are also excluded; 6C*0106+397 does not cover the wavelength of the redshifted Lyα and 6C*0041+469 lacks sufficient signal-to-noise. Qualitatively, the spectra of the excluded 3CRR, 6CE sources and 6C*0106+397 look similar to the composites, so no bias is expected. The few weak-line objects (6C*0041+469, 5C6.242, 5C7.208) are not concentrated in one bin in D and so should not seriously skew the result.

We found a factor of ~ 1.7 higher CII]$\lambda 2326$ Å flux in sources with $\log_{10} L_{151} > 27.5$ than for sources at $\log_{10} L_{151} < 27.5$. However, there was no discernible difference between the CIV$\lambda 1549$ Å and HeII$\lambda 1640$ Å line fluxes in the two bins. Thus, we conclude that there is no *strong* correlation between the low-frequency radio luminosity and the ionisation state of the emission-line region. This is in agreement with the results of Tadhunter et al. (1998) for a low-redshift sample ($z < 0.7$) of 2 Jy radio sources, where they also found no evidence for a correlation between ionisation state measured by the ratio of [OII]$\lambda 3727$ / [OIII]$\lambda 5007$ and radio luminosity. If any such correlation exists it may well be best seen amongst the sources with the lowest photoionising power Q_{phot} in complete samples (Saunders et al. 1989); in Fig. 8, the luminosity of all lines even those of low luminosity like [OII] scale with incident photoionising luminosity. However, Stern et al. (1999) have found a very tentative correlation between CIV / CIII] ratio and radio luminosity within a sample of 30 radio galaxies, mainly from the MIT-Green Bank survey (Bennett et al. 1986; Lawrence et al. 1986) and the ultra-steep sample of Röttgering et al. (1994). However, this correlation is extremely weak, being significant at the $\approx 2\sigma$ level. This correlation was also not seen in the work of De Breuck et al. (2000b) and should be viewed with caution.

Returning to the sub-sample of 35 objects from our dataset considered in Sec. 6.1 we also find a highly tentative correlation between the residual Lyα emission-line luminosity (after subtraction of the $L_{\mathrm{Ly}\alpha}$ calculated from the radio luminosity of each source using the best-fit derived in Sec. 6.1) and the projected linear size of the radio sources in our dataset. The Spearman rank coefficient for this correlation is $r_{\mathrm{s}} \approx 0.23$, with the two-tailed probability that this arises by chance, given the null hypothesis of no correlation of $P_{\mathrm{r}} \approx 17\%$ for the best-fit with all sources included. If 5C7.271 and 6C*0135+313 are excluded then the correlation becomes slightly more significant with $r_{\mathrm{s}} \approx 0.27$ with $P_{\mathrm{r}} \approx 13\%$.

Although normally we would be highly suspicious of what is clearly a marginal correlation, we will explore a physical model in Sec. 7 involving the quantity $\Theta \equiv L_{\mathrm{Ly}\alpha}/L_{151}^{6/7}$ (the form of the residual after taking out the correlation of Fig. 5 as detailed in Sec. 6.1). We plot $\log_{10}\Theta$ against $\log_{10}D$ in Fig. 7. With our dataset combined with the sources from De Breuck et al. (2000b) the correlation between Θ and D is significant at the 94% level ($r_{\mathrm{s}} \approx 0.19$), with a best fit slope of 0.55 ± 0.10. Although evidence for a positive correlation in Fig. 7 is slight, it is interesting in the light of the weak but significant (at the 99% level) *negative* correlation seen in the plot of residual [OII] luminosity versus D in Willott et al. (1999).

One explanation of this difference is that the smaller sources have stronger associated HI absorption (van Ojik et al. 1997) and hence, systematically suppressed Lyα than in the larger sources. Indeed, van Ojik et al. (1997) found that 90% of small (< 50 kpc) radio galaxies have strong associated absorption, whereas only 25% of the larger (> 50 kpc) radio galaxies exhibit such strong absorption. Our spectroscopic dataset has insufficient resolution and sensitivity to check this result with the combined 3CRR, 6CE, 7CRS and 6C* samples. However, if we assume that approximately 50% of the Lyα flux is absorbed for sources with $D \leq 50$ kpc (van Ojik et al. 1997), then the correlation of Fig. 7 could be weakened or extinguished. To test this, we doubled the Lyα fluxes of all sources with $D \lesssim 50$ kpc and recalculated the correlations finding the significance of the combined sample drops to $\sim 60\%$ with a best-fit slope of ≈ -0.2. We conclude that HI absorption is a plausible source of the weak positive correlation in Fig. 7, but it does not explain why residual [OII] shows an anti-correlation with D.

Why then do Willott et al. (1999) find an anti-correlation between the residual [OII] luminosity (after taking out the strong $L_{\mathrm{[OII]}} - L_{151}$ correlation) and D? One possible reason is that we do not yet have enough data to strengthen the correlation, both from a lack of high resolution spectroscopy around the Lyα emission-line to constrain the HI absorption, and from the intrinsically small dataset of sources at $z > 1.75$. However, assuming that this is not the case, and that our small sample is representative of the population as a whole, we conclude this section by developing a physical argument to explain this.

Note first that our study finds tentative evidence that, at a given L_{151} at $z > 1.75$, the smallest ($D \lesssim 70$ kpc) radio sources have relatively low line luminosities of lines like Lyα (and HeII and CIV): the evidence for systematically low Lyα luminosity comes from the correlation of Fig. 7 and for low CIV/HeII luminosities from Fig. 6 and Table 5. Since in the absence of HI absorption Lyα tracks Q_{phot} (see Fig. 8), this is in qualitative agreement with simple radio source models (e.g. Willott et al. 1999) in which the smallest sources (of a given L_{151}) are young objects of systematically lower Q than their older (larger D) counterparts, and in which the photoionising power faithfully tracks Q which is assumed to be independent of radio source age (see Sec. 7).

Note second that the relative strength of low-ionisation lines like CII] and [OII]$^{\|}$ in the small (low D) sources can then be viewed as a boosted low-ionisation

---

component. From our Fig. 6 and Table 5, and Fig. 4 of Willott et al. (1999), and indeed Fig. 1 of Best et al. (2000), we can infer that the flux from low-ionisation lines needs to be boosted by a factor ~ 5. It seems plausible that this can be achieved by compressing and potentially shredding emission-line clouds, as the source passes through radii $\lesssim 50$ kpc, decreasing the U_e at each cloud and potentially increasing the covering factor for photoionising radiation from the nucleus (see e.g. Bremer, Fabian & Crawford 1997). As illustrated by Fig. 8, the ratio of [OII]/Lyα increases by about the required factor if U_e drops from about 10^{-2} to 10^{-3} due to compression of the gas clouds by a factor ~ 10 within the photoionising cone of the quasar (e.g. Lacy et al. 1998). Although the radio source induced shocks could also yield in situ photoionisation (e.g. Dopita & Sutherland 1996; Best et al. 2000) these would in general boost all narrow-line emission and do not seem to be required by the data. The negative correlation between D and the FWHM of [OII] (Best et al. 2000) show that the shocks do appear to be affecting the kinematics of the line-emitting clouds. Kaiser, Schoenmakers & Röttgering (2000) argue that clouds like those we deem to be responsible for the boosted low-ionisation component will disperse as the radio source propagates to larger radii; the data of Best et al. on large-D 3C sources (namely line widths appropriate to gravitationally-induced motions and simple quasar-excited line ratios) are in accord with this picture.

The complicating effects on line ratios introduced by H I absorption and/or radio source induced changes in U_e mean that it is probably dangerous to use a single emission line to measure Q_{phot}. It is not surprising that the details of emission line/radio correlations appear to depend on the line studied. As advocated by Rawlings & Saunders (1991), an estimate of total line-luminosity (ideally by summing the flux from all of the narrow emission lines and accounting for absorption and reddening) is required to probe, for example, the true slope of the emission line/radio correlation - but the requisite comprehensive UV/optical/near-infrared dataset is not yet available for samples of radio sources.

6.3 Radio source size and the extent of the Lyα emission-line region

We now investigate whether there is a link between the size of the radio source and that of the Lyα emission-line region which might be expected if the radio source itself is capable of producing additional UV opaque material at radii $\lesssim 50$ kpc (e.g. via the shredding mechanism of Bremer et al. 1997). The extent of the Lyα emission line was measured at the full-width zero-intensity of a cross-cut through the emission line for all sources for which we have 2-D spectra and deconvolving them from the seeing [Sec. 3 for the 6C* sources; Rawlings

Emission line ID	λ (Å)	$D < 70$ kpc (% of Lyα)	$D > 70$ kpc (% of Lyα)
Lyα	1216	100	100
CIV	1549	7 ± 1	14 ± 2
HeII	1640	4 ± 2	20 ± 2
CIII]	1909	5 ± 2	4 ± 1
CII]	2326	10 ± 2	3 ± 1
NeIV	2424	4 ± 2	2 ± 1

Table 5: Emission line ratios to Lyα for our composite radio galaxy spectra (Fig. 6) for radio galaxies with $D < 70$ kpc and $D > 70$ kpc. The uncertainties on the ratios are $\approx 1\sigma$ errors and arise from several factors, e.g. the uncertainties of the continuum level.
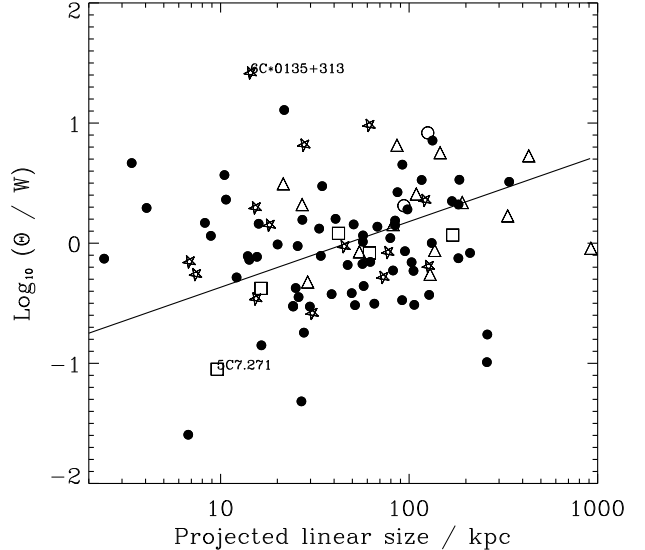

Figure 7: The residual emission-line luminosity (after subtraction of the best-fit $\log_{10} L_{\text{Ly}\alpha} - \log_{10} L_{151}$ slope of Fig. 5) against projected linear size of the radio galaxies from our 3CRR (open circles), 6CE (triangles), 7CRS (squares) and 6C* (stars) datasets combined with that of De Breuck et al. (2000b) (filled circles). The solid line shows the best-fit to the data.

et al. (2001) for the 6CE sources][**]. Our results are illustrated in Fig. 9 where we plot the extent of the Lyα region along the slit versus the projected linear size of the radio source. It is apparent that there exists a strong correlation between the extent of the Lyα emission and the projected size of the radio source, with a $r_e = 0.54$

[**] 26 of the 38 objects in our dataset are included: sources excluded because the 2D spectra are unavailable are all those from the 3CRR and 7CRS samples, and for the same 6CE and 6C* sources excluded from the composite spectra of Fig. 6; namely, 6CE0902+3419, 6CE1141+3525 and 6CE1232+3942 from the 6CE sample and 6C*0106+397 from 6C*.
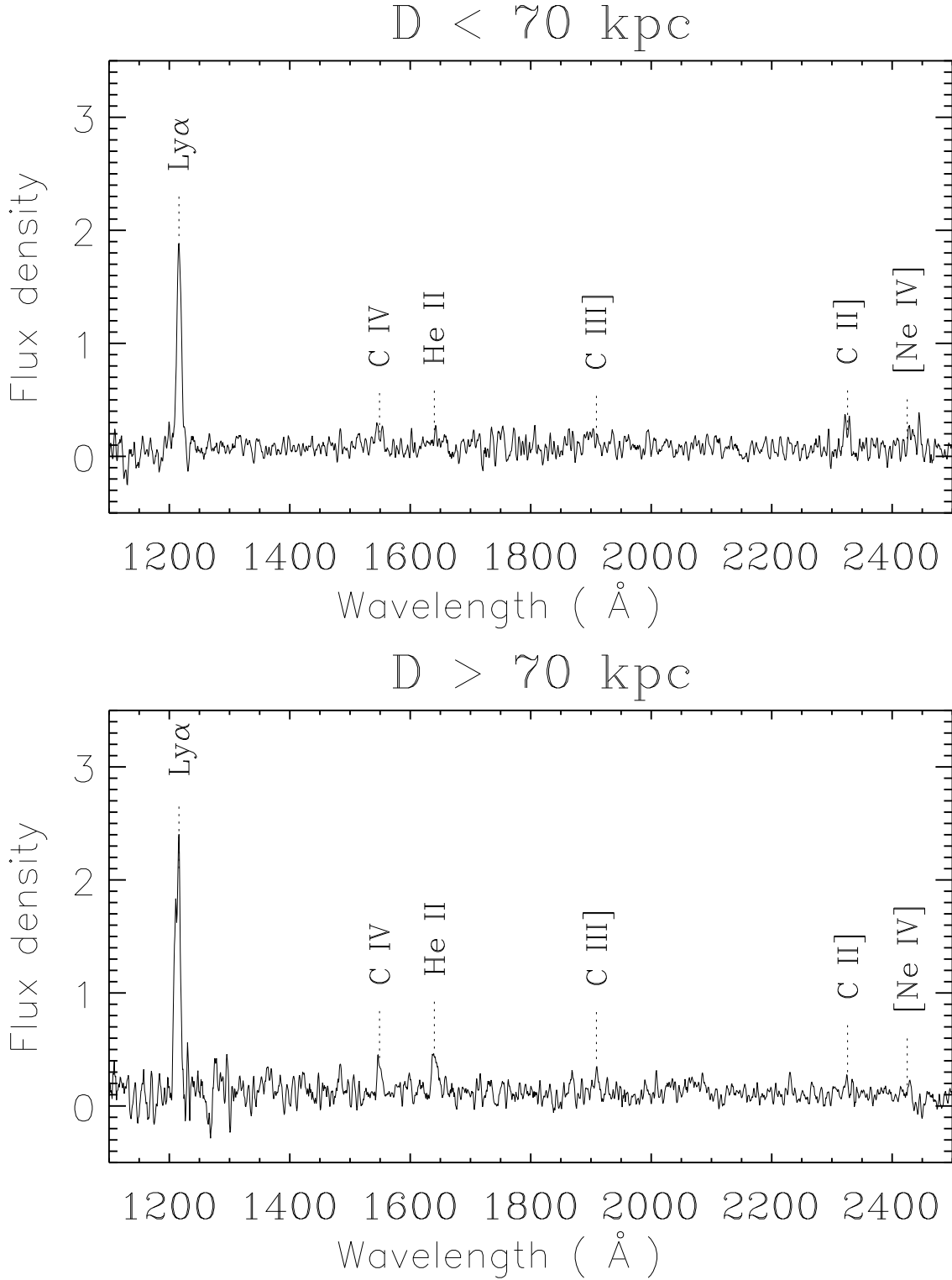
Figure 6: Composite spectra resulting from 14 sources (8 from 6C*, 2 from 6CE and 4 from 7CRS) with projected linear sizes $D < 70$ kpc (top) and 13 (4 from 6C*, 8 from 6CE and 1 from 7CRS) sources with $D > 70$ kpc (bottom). Only the sources with Lyα in the spectrum were used as the integrated Lyα flux was used to normalise the different spectra, the method of combination is that described in Rawlings et al. (2001) and the resultant spectrum has been smoothed with a 3-bin boxcar filter. The flux-density is measured in units of W m^{-2} Å^{-1} with an arbitrary normalisation.
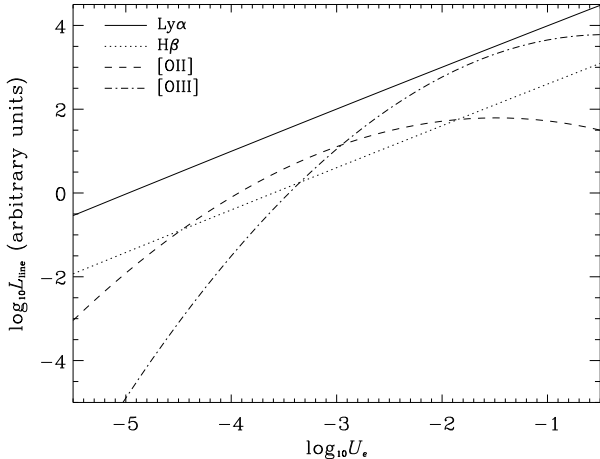
Figure 8: Luminosity of the Lyα (solid line), Hβ (dotted line), [OII] (dashed line) and [OIII] (dotted-dashed line) emission lines as a function of effective ionisation parameter, U_e for an ionisation-bound plane-parallel slab with a hydrogen number density of $10^9 \, \mathrm{m}^{-3}$; U_e is given as the ratio of the photon number density to particle number density at the incident face of the cloud, i.e. $U_e = Q_{\mathrm{phot}}/(4\pi r^2 cn)$, where r is the distance to the cloud from the ionising source and n is the particle density. This was modelled with CLOUDY Version 94.00 (van Hoof, Martin & Ferland 1999; **http://www.pa.uky.edu/∼gary/cloudy/**) using the AGN continuum spectrum described by Mathews & Ferland (1987), for Lyα, Hβ, [OII] and [OIII]. Both Lyα and Hβ respond linearly to increases in the effective ionisation parameter U_e, so that if quasars of all luminosities had narrow-line regions with similar radial density profiles then one might expect a proportionality between $L_{\mathrm{Ly}\alpha}$ (or $L_{\mathrm{H}\beta}$) and quasar luminosity over the full range in the photoionising luminosity Q_{phot}, although (as will be discussed in Sec. 6.3) it should be noted that the CLOUDY-based modelling takes no account of the resonant HI absorption of Lyα.

with a 0.5% probability of this correlation occurring by chance. This is in agreement with previous work addressing this by van Ojik et al. (1997) for objects at $z > 2.1$, although the majority of their objects (which are also plotted in Fig. 9) lie above our best-fit to the correlation (Fig. 9). There are two possible reasons for this. First, the sample of van Ojik et al. is not complete in the sense of the 3CRR, 6CE and 7CRS samples, and does not have the well defined filtering criteria of the 6C* sample: their sample was selected on the basis of bright Lyα emission lines and there is an obvious danger of them missing compact low-luminosity Lyα emitters. Second, the length of our exposures, which were kept relatively short to permit more pointings in a single observing run, might have led to some of the Lyα flux falling below our detection limit.

The results of Fig. 9 are in agreement with the idea

that additional UV-opaque emission line material is produced at radii $\leq 50 \, \mathrm{kpc}$ by interactions between the expanding radio source and its environment. For linear sizes in the range $10 \leq D \leq 100 \, \mathrm{kpc}$ the sizes of the corresponding Lyα emitting regions are scattered up to a maximum value which closely tracks the size of the radio source, and thus provides the envelope driving the correlation.

There are two 6C* sources (6C*0135+313 and 6C*0208+344) which appear to lie clearly above the envelope given by the (dotted) line of equality in Fig. 9 [One of these (6C*0135+313) was the prominent outlier noted in Fig. 5.] These both lie at sufficiently low values of D that it is certainly plausible that there is sufficient dense narrow-line material at the radii in question to produce detectable Lyα emission before any boosting effects caused by the expanding radio source (see also van Ojik et al. 1997). In the case of 6C*0135+313, detection of Lyα at large radii (for a small D source) might be linked to the anomalous high Lyα luminosity of this source (Fig. 5).

The existence of at least one $D \sim 100 \, \mathrm{kpc}$ source with a compact region is also not too surprising: the size of the Lyα emitting region will clearly involve a competition between narrow-line covering factor enhancement processes (e.g. Bremer et al. 1997) and reduction processes (e.g. Kaiser et al. 2000) which might be expected to vary considerably from source-to-source given perhaps only subtle environmental differences. We expect from the results of Best et al. (2000) that the correlation between Lyα size and D will break down at $D \geq 100 \, \mathrm{kpc}$, presumably because of the absence of the seed material for luminous narrow-line clouds at very large radii.

7   THE IMPORTANCE OF SOURCE AGE OVER ENVIRONMENT

In this section we develop an argument based on the correlations discussed in Secs. 6.1, 6.2 & 6.3 which suggests that source age has a much more profound influence on radio source properties than environment.

We adopt the simple model[††] for radio source evolution used by Willott et al. (1999), including an assumed power-law environmental density profile $n(r)$ given by

$$n(r) = n_{100} \left(\frac{r}{100\mathrm{kpc}} \right)^{-\beta}, \tag{1}$$

where $\beta \simeq 1.5$ and is a dimensionless parameter. In

---

[††] More complicated models exist which account for synchrotron and inverse-Compton cooling (e.g Kaiser, Dennett-Thorpe & Alexander 1997), and the rôle of the hotspot in governing the electron energy spectrum injected into the lobe (Blundell et al. 1999), but for sources in the flux-density limited samples this simple model suffices.
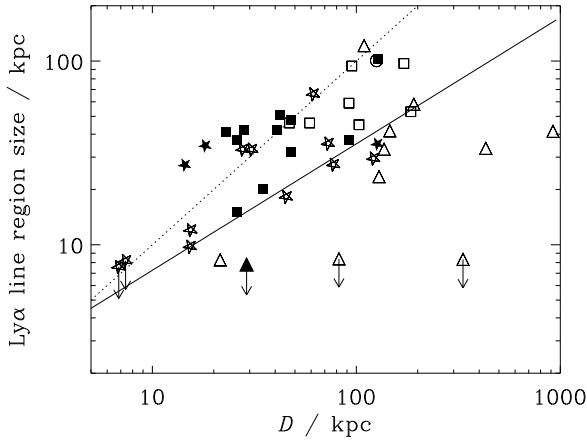
Figure 9: The extent of the Lyα emission line region versus projected radio size. The 6C* objects are denoted by the stars; the 6CE objects by triangles; and 3CRR by circles. The squares are the points of van Ojik et al. (1997). The objects with strong associated absorption are denoted by the filled symbols. The solid line is the best-fit to our data. The dotted line is the line of equality between the Lyα extent and D. Note that two 6C* sources (6C*0135+313 and 6C*0208+344) are significantly above this line implying that the extent of the Lyα emission exceeds the extent of the radio emission. It is interesting to note that these two sources both appear to exhibit HI absorption. The 6CE source with associated absorption is 6CE0930+3855 (Rawlings et al. 2001). Note that the upper limit symbols mean that the emission line detections are unresolved in our data.

addition to the normalising factor n_{100}, the other key physical variables influencing the evolution of a radio source are bulk jet power Q and source age t. These are linked to the observables L_{151} and D via the equations

$$D \propto \left(\frac{t^3 Q}{n_{100}}\right)^{\frac{1}{5-\beta}} \propto Q^{2/7} n_{100}^{-2/7} t^{6/7} \quad \text{(for } \beta = 1.5\text{)} \qquad (2)$$

$$L_{151} \propto Q^{(26-7\beta)/[4(5-\beta)]} n_{100}^{9/[4(5-\beta)]} t^{(8-7\beta)/[4(5-\beta)]} \qquad (3)$$
$$\propto Q^{31/28} n_{100}^{9/14} t^{-5/28} \quad \text{(for } \beta = 1.5\text{)}.$$

The physical basis for these equations are the dimensional arguments of Falle (1991), and energy conservation (assuming Q to be independent of t) following the ideas of Scheuer (1974) [see Willott et al. (1999) and Blundell & Rawlings (1999) for further details].

If we add to this model the assumption that $Q \propto Q_{\text{phot}} \propto L_{\text{Ly}\alpha}$ [e.g. Rawlings & Saunders (1991), Willott et al. (1999) and Fig. 8] we can combine eqns. 2 & 3 to show that

$$\Theta \equiv \frac{L_{\text{Ly}\alpha}}{L_{151}^{6/7}} \propto D^{5/28} n_{100}^{-1/2}, \qquad (4)$$

where our discussion of Sec. 6.2 shows that the log of the

left-hand side of this equation is essentially the residual Lyα quantity plotted against D in Fig. 7.

The tentative correlation seen in Fig. 7 is in quantitative agreement with the slow dependence of Θ on D [within the uncertainties, e.g. including some correction for HI absorption (Sec. 6.3), the slope is $\sim 5/28$]. We can then conclude that the range in n_{100} cannot be so large that it would disrupt this correlation, i.e. $\Delta n_{100} \leq 50$. Although the existence of any $\Theta - D$ correlation due to these effects is highly tentative (see discussion of HI absorption effects in Sec. 6.2) the data in Fig. 7 are consistent with a very gradual dependence of Θ on D and require a restricted range in density n_{e}.

We are therefore led to a picture in which all $z > 1.75$ luminous radio galaxies have similar environments (and values of n_{100}). Thus, as a source ages, the linear size D is driven largely by the time dependence in eqn. 2 so that the spread in D is dominated by the spread in ages, which for the low-frequency selected objects in question mean ~ 2 dex spread in Fig. 7. L_{151} drops slowly with age (eqn. 3) so, at a given L_{151}, the smallest sources will be drawn from objects with a lower Q and have lower Lyα: this is a possible origin for the tentative correlation between Θ and D in Fig. 7. As the shocks pass through the $r \lesssim 50$ kpc region, compression of cool clouds (e.g. Lacy et al. 1998) will temporarily increase the ratios of lines like [OII] and CII] to Lyα, thus explaining the anti-correlation of residual [OII] and D (Willott et al. 1999), the differences between the composite spectra in Fig. 6 (Table 5) and the results of Best et al. (2000). Shredding of emission-line clouds can increase the effective covering factor, producing a moderate amount of additional extended Lyα emission. This explains the correlation between Lyα size and D in Fig. 9. As the source passes to $D \gtrsim 100$ kpc the seed material for the clouds is now completely contained within the high-pressure radio lobes, and as argued by Binette et al. (2000) the clouds which condense are not dense enough, or too far from the ionising nucleus, to produce detectable Lyα emission; they will also shadow too small a fraction of the inner Lyα emission to produce detectable HI absorption.

Despite our data agreeing in all important respects with those of van Ojik et al. (1997) we reach an opposite conclusion. They favour an environmental/frustrated scenario in which the smallest high-redshift radio sources reside in the densest (e.g. cluster) environments. While we cannot rule out subtle effects of this type, we have argued that the variation in the age of radio sources is the dominant effect on its size, and variations in age, not environment are (after Q) the most important drivers of the emission line properties.

The main argument used by van Ojik et al. (1997) against the scenario we now prefer was a perceived difficulty explaining the decrease in HI absorption as the radio source propagates to large D. As Binette et al. (2000) have recently argued, this was probably because

van Ojik et al. (1997) assumed that the emission and absorption gas was co-spatial with similar physical conditions. Binette et al. (2000) present a compelling argument that absorption is caused by ionised material in an outer halo which may well provide the seed material for Lyα-emitting gas, but which has a much lower density and much higher filling factor prior to the passage of the radio source shocks.

Our contention that variations in source age are more important than variations in source environment has some interesting implications. First, it fits in naturally with the explanation for the well-known anti-correlation between D and z preferred by Blundell et al. (1999) and Blundell & Rawlings (1999) - the so-called 'youth-redshift degeneracy' - and argues against the 'evolving environments' explanation preferred by Neeser et al. (1995). Second, it suggests that there is not a significant spread in the environmental properties amongst luminous high-redshift radio galaxies. It should be noted that Bremer et al. (1997) reach similar conclusions from their starting hypothesis that luminous radio sources inhabit the central regions of massive cooling-flow clusters.

Irrespective of the details, our broad conclusion is perhaps not too surprising. The hypothesis that radio galaxies pinpoint recently collapsed structures is not new (e.g. Haehnelt & Rees 1993), and since the density inside such systems depends only on the epoch of collapse, the small range in z probed by this and similar studies should yield only a small variation in environmental properties.

8   CONCLUSIONS

In this section we reiterate our main conclusions derived from new studies made possible by the 6C* sample.

• The filtering criteria and flux-density limits employed in the 6C* sample to find objects at $z > 4$ are such that the fraction of high-redshift objects is significantly larger than if no filtering were employed, and this allowed the discovery of 6C*0140+326 at $z = 4.41$ and 6C*0032+412 at $z = 3.66$. The median redshift of the 6C* sample is ~ 1.9 whereas the median redshift of a complete sample at the flux-density of 6C* is ~ 1.1.

• We find a rough proportionality between the luminosity of the narrow Lyα emission line $L_{\mathrm{Ly}\alpha}$ and the rest-frame 151-MHz radio luminosity L_{151}, for sources at $z > 1.75$. This correlation is similar to that found by Willott et al. (1999) for the luminosity of [OII] versus L_{151} for radio sources and may be interpreted in the same way, namely as evidence for a primary relationship between the accretion rate and the jet power of radio sources (Rawlings & Saunders 1991; Willott et al. 1999).

• We present tentative evidence that high-redshift radio sources with large projected linear sizes ($D >$ 70 kpc) have higher ionisation states than their smaller counterparts. This is in agreement with the work of Best et al. (2000) for similarly radio luminous 3CRR radio sources at $z \sim 1$.

• We find a weak correlation between residual $L_{\mathrm{Ly}\alpha}$ (having corrected for the strong correlation between $L_{\mathrm{Ly}\alpha}$ and L_{151}) and D, whereas previous work on samples with a lower median-redshift (Willott et al. 1999) found a weak anti-correlation between the residual luminosity of [OII] and the size of the radio source. This may be explained in two ways: (i) the smaller sources have stronger associated absorption of Lyα than the larger sources, and (ii) the slope of the residual $L_{\mathrm{Ly}\alpha} - D$ is similar to the power-law dependency of radio jet-power on radio source size from simple evolutionary models of radio sources (Willott et al. 1999). If effect (ii) is real then the Lyα luminosity seems to trace the underlying ionising continuum much better than [OII], which may be boosted in small sources by compressions associated with shocks caused by the radio source as it propagates through regions close ($\lesssim 50$ kpc) to the nucleus.

• There exists a strong correlation between the size of the Lyα emission region and the size of the radio source in the sense that the total Lyα size is $\lesssim D$ for $D \lesssim 100$ kpc. This suggests that extra Lyα in emission is being promoted by the expansion of the radio source, perhaps via a shredding mechanism (Bremer et al. 1997) which increases the covering factor to quasar radiation from the nucleus.

• We combine the observational results to develop an argument that suggests variations in source age have a stronger influence on the radio/emission-line properties of high-redshift radio luminous galaxies than variations in environment. A small range in environmental properties is deduced which is in line with the hypothesis that luminous high-redshift radio sources are triggered in recently collapsed massive structures.

REFERENCES

Bennett C.L., Lawrence C.R., Burke B.F., Hewitt J.N., Mahoney J., 1986, ApJS, 61, 1

Best P.N., Röttgering H.J.A., Longair M.S., 2000, MNRAS, 311, 23

Bicknell G.V., Dopita M.A., O'Dea C.P.O., ApJ, 1997, 485, 112

Binette L., Kurk J.D., Villar-Martin M., Röttgering H.J.A., 2000, A&A, 356, 23

Blundell K.M. & Rawlings S., 1999, Nature, 399, 330

Blundell K.M., Rawlings S., Eales S.A., Taylor G.B., Bradley A.D., 1998, MNRAS, 295, 265

Blundell K.M., Rawlings S., Willott C.J., 1999, AJ, 117, 677

Bremer M.N., Fabian A.C., Crawford C.S., 1997, MNRAS, 284, 213

Chambers K.C., Miley G.K., van Breugel W.J.M., 1990, ApJ, 363, 21

Chambers K.C., Miley G.K., van Breugel W.J.M., Huang J.-S., 1996, ApJS, 106, 215

Condon J.J., Cotton W.D., Greisen E.W., Yin Q.F., Perley R.A., Taylor G.B., Broderick J.J., 1998, AJ, 115, 1693

De Breuck C., 2000c, Very Distant Radio Galaxies, PhD. Thesis, University of Leiden

De Breuck C., van Breugel W., Röttgering H.J.A., Miley G., 2000a, A&AS, 143, 303

De Breuck C., Röttgering H., Miley G., van Breugel W., Best P., 2000b, A&A, 362, 519

de Ruiter H.R., Parma P., Fanti C., Fanti R., 1986, AASS, 65, 111

Dopita M.A., Sutherland R.S., 1996, ApJSS, 102, 161

Douglas J.N., Bash F.N., Bozyan F.A., Torrence G.W., Wolfe C., 1996, AJ, 111, 1945

Dunlop J.S.& Peacock J.A., 1990, MNRAS, 247, 19

Eales S.A., Rawlings S., 1993, ApJ, 411, 67

Egami E., Armus L., Neugebauer G., Soifer B.T., Evans A.S., Murphy T.W., 1999, in The Hy-redshift universe: Galaxy formation and evolution at high redshift' eds. A.J. Bunker and W.J.M. van Breugel

Falcke H. & Biermann P.L., 1995, A&A, 293, 665

Falle S.A.E.G., 1991, MNRAS, 250, 581

Fanti C., et al., 2000, A&A, 358, 499

Gopal-Krishna, Wiita P.J., 1996, ApJ, 467, 191

Haehnelt M.G., Rees M.J., 1993, MNRAS, 263, 168

Hales S.E.G., Baldwin J.E., Warner P.J., 1993, MNRAS, 263, 25

Jarvis M.J., 2000, The Most Distant Radio Galaxies, PhD thesis, University of Oxford

Jarvis M.J., Rawlings S., Willott C.J., Blundell K.M., Eales S.A., Lacy M., 2001a, MNRAS submitted

Jarvis M.J., Rawlings S., Eales S.A., Blundell K.M., Bunker A.J., Croft S.D., McLure R.J., Willott C.J., 2001b, MNRAS submitted (Jea01)

Jaynes E.T., 1991, Straight Line Fitting - A Bayesian Solution, unpublished manuscript, http://bayes.wustl.edu/etj/node2.html

Kaiser C.R., Dennett-Thorpe J., Alexander P., 1997, MNRAS, 292, 723

Kaiser C.R., Schoenmakers A.P., Röttgering H.J.A., 2000, MNRAS, 315, 381

Koekemoer A.M., Bicknell G.V., 1998, ApJ, 497, 662

Lacy et al., 1994, MNRAS, 271, 504

Lacy M., Rawlings S., Blundell K.M., Ridgway S.E., 1998, MNRAS, 298, 966

Laing R.A., Riley J.M. & Longair M.S., 1983, MNRAS, 204, 151

Lawrence C.R., Readhead A.C.S., Moffett A.T., Birkinshaw M., 1986, ApJS, 61, 105

Macklin J.T., 1982, MNRAS, 199, 1119

Mathews W. G., Ferland G. J., 1987, ApJ, 323, 456

McCarthy P.J., 1993, ARAA, 31, 639

McCarthy P.J., van Breugel W., Kapahi V.K., 1991, ApJ, 371, 478

Miller J.S., Stone R.P.S., 1994, Lick Obs. Tech. Reports, vol.66

Neeser M.J., Eales S.A., Law-Green J.D., Leahy P.J., Rawlings S., 1995, ApJ, 451, 76

Oke J.B. et al., 1995, PASP, 107, 375

Rawlings S., Eales S.A., Lacy M., 2001, MNRAS, 322, 536

Rawlings S., Lacy M., Blundell K.M., Eales S.A., Bunker A.J., Garrington S.T., 1996, Nature, 383, 502

Rawlings S., Saunders R., 1991, Nature, 349, 138

Rhee G., Marvel K., Wilson T., Roland J., Bremer M., Jackson N., Webb J., 1996, ApJSS, 107, 175

Röttgering H.J.A., Lacy M., Miley G.K., Chambers K.C., Saunders R., 1994, A&AS, 108, 79

Saunders R., Baldwin J.E., Rawlings S., Warner P.J., Miller L., 1989, MNRAS, 238, 777

Scheuer P.A.G., 1974, MNRAS, 166, 513

Simpson C., 1998, MNRAS, 297, L39

Singal A.K., 1993, MNRAS, 262, L27

Stern D., Dey A., Spinrad H., Maxfield L., Dickinson M., Schlegel D. González R. 1999, AJ, 117, 1122

Tadhunter C.N., Morganti R., Robinson A., Dickson R., Villar-Martin M., Fosbury R.A.E., 1998, MNRAS, 298, 1035

van Hoof P.A.M., Martin P.G., Ferland G.J., o appear in Cosmic Evolution and Galaxy Formation: Structure, Interactions, and Feedback, ASP Conference Series, J. Franco, E. Terlevich, O. Lopez-Cruz and I. Aretxaga, eds. (extended version) (astro-ph/0001196)

van Ojik R., Röttgering H.J.A., Miley G.K., Hunstead R.W., 1997, A&A, 317, 358

Willott C.J., 2000, to appear in AGN in their cosmic environment eds. B. Rocca-Volmerange and H. Sol

Willott C.J., Rawlings S., Blundell K.M., 2001b, MNRAS in press. (astro-ph/0011082)

Willott C.J., Rawlings S., Blundell K.M., Lacy M., 1999, MNRAS, 309, 1017

Willott C.J., Rawlings S., Blundell K.M., Lacy M., 2000b, MNRAS, 316, 449

Willott C.J., Rawlings S., Blundell K.M., Lacy M., Eales S.A., 2001a, MNRAS, 322, 536

Willott C.J. Rawlings S. & Jarvis M.J., 2000a, MNRAS, 313, 237

APPENDIX : SOURCES EXCLUDED FROM 6C*

We show in Figs. 11 & 12 NVSS radio maps of the five radio sources from the original 6C* sample excluded from the final version because their angular sizes are now known to be > 15 arcsec. We also present 1-D optical spectra for three of these sources (Fig. 13 & 14) taken before it was clear that their true angular sizes exceeded the $\theta < 15$ arcsec filtering criterion of the 6C* sample.

6C*0100+312 This source is a quasar at $z = 1.189$ (see Fig. 13), but is excluded from the 6C* sample as the angular size of the radio source is ≈ 90 arcsec [Fig. 11 and the radio map in Blundell et al. (1998)].

6C*0107+448 Our 8.4 GHz map of this sources (Blundell et al. 1998) revealed radio structure with four components on a scale $\lesssim 10$ arcsec. The NVSS map suggested that these components may be part of a radio lobe of a large (1.5 arcmin) double radio source. How-

ever, a deep $R-$band image revealed emission co-spatial with the bright radio component in our 8.4 GHz and led us to believe that it was indeed an isolated source. Spectroscopy failed to resolve the redshift of the source, however continuum and a strong emission line were observed, which we associated with the faint $R-$band object. A subsequent radio map at 1.4 GHz (Jea01) has now revealed that this source is indeed a large classical double and the emission we see in our optical imaging data is either associated with the hot-spot or a foreground object.

6C*0111+367 We have now determined that the brightest component on the original 4.9 GHz radio map (Blundell et al. 1998) is a hot-spot associated with a larger source. The faint radio emission in the 8.4 GHz map is now identified with an object on our R-band image (Jea01) at 01 11 29.8 +36 43 27.5 (B1950), and we take this as the core, the other weak feature on the 8.4 GHz map at 01 11 27.8 +36 43 19.0 (B1950) is now assumed to be a second lobe as these three components are roughly co-linear. Thus, the radio structure is $\approx$ 41 arcsec; its redshift is unknown.

6C*0120+329 This source has an angular size $\theta \approx$ 95 arcsec (Parma et al. 1986), so is excluded from the sample. The redshift of this source is $z = 0.0164$ (de Ruiter et al. 1986).

6C*0141+425 Blundell et al. (1998) mentioned that this is possibly a double radio source with $\theta \approx$ 113 arcsec and the NVSS map confirms this. The redshift of this source is $z = 0.0508$ and the 1-D spectrum is presented in Fig. 14.
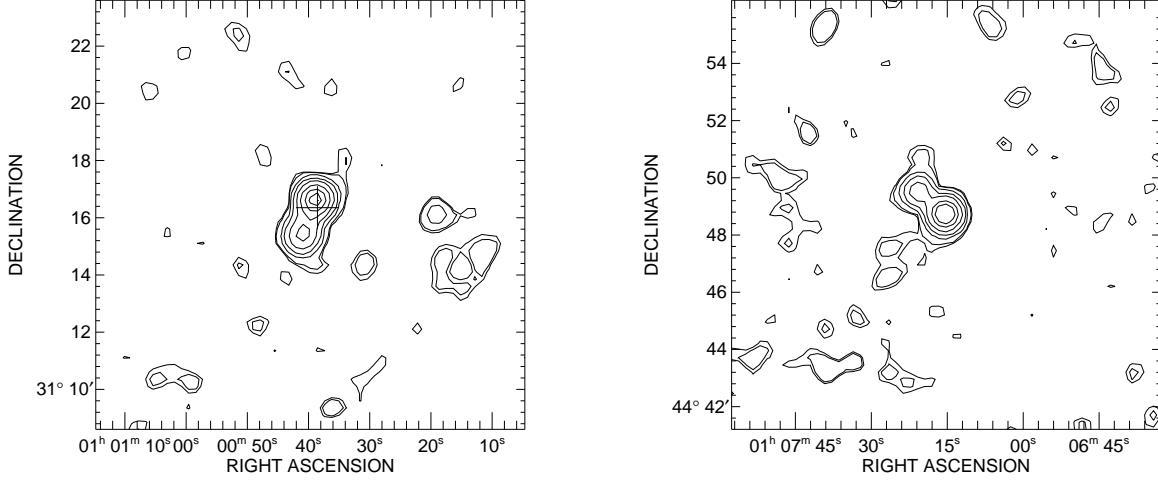
Figure 10: NVSS radio maps of two 6C* radio sources excluded from the final sample; the cross marks the optical positions. 6C*0100+312 (left) is now identified with a quasar (Fig. 13) with an angular size of ≈ 1.5 arcmin from our 1.5 GHz map (Blundell et al. 1998). The NVSS 1.4 GHz map shown resolves the source with the 45 arcsec beam and has a peak flux of 63.7 mJy/beam (contour levels in mJy per synthesised beam are 62, 50, 35, 20, 10, 5, 2.5, 1, 0.75). 6C*0107+448 (right), the optical identification for this source is still ambiguous from our $R-$ and $K-$band images and the digitised sky survey, with no obvious bright identification. This ≈ 1.5 arcmin source has a peak flux of 50.8 mJy/beam (contour levels in mJy per synthesised beam are 45, 38, 32, 26, 20, 14, 7, 2).
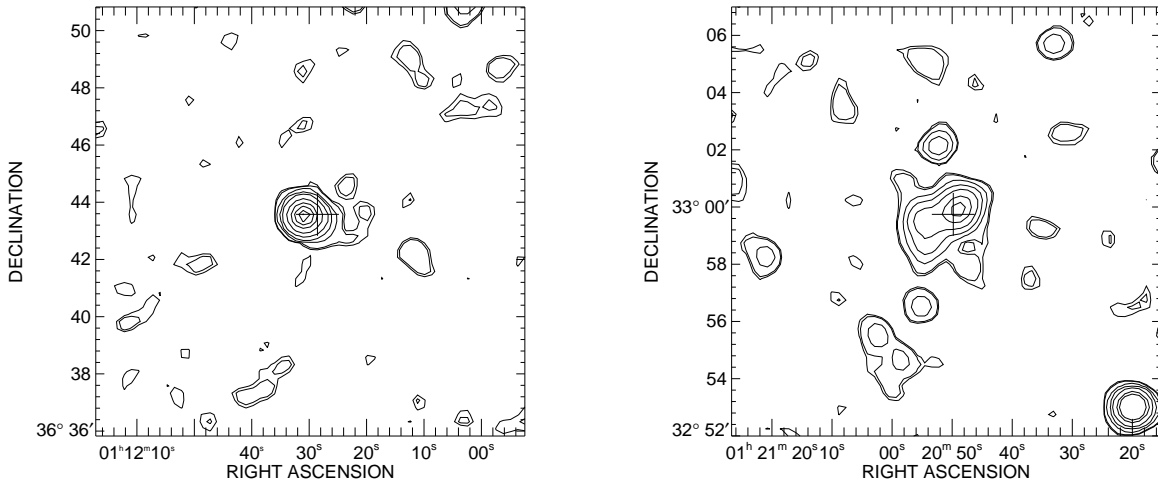

Figure 11: NVSS radio maps of two 6C* radio sources excluded from the final sample; the crosses mark the optical positions. 6C*0111+367 (left) is resolved in this NVSS map and our 1.49 GHz map suggests an angular size of ≈ 41 arcsec, it has a peak flux of 123.9 mJy/beam (contour levels in mJy per synthesised beam are 120, 100, 75, 50, 25, 10, 5, 2.5, 1, 0.75). 6C*0120+329 (right) is resolved with the 45 arcsec beam of NVSS and has a peak flux of 36.4 mJy/beam (contour levels in mJy per synthesised beam are 30, 20, 10, 5, 2.5, 1, 0.75).
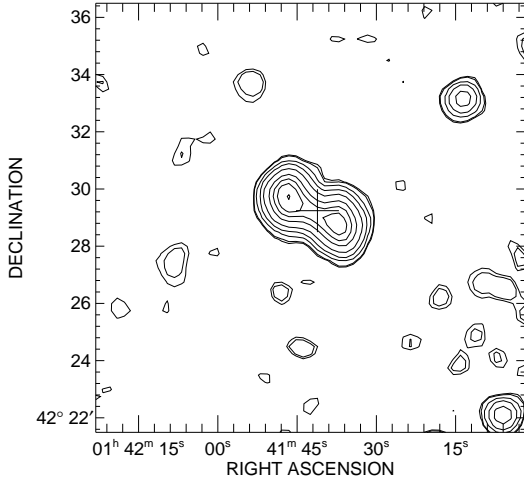
Figure 12: 6C*0141+425 (right) is also resolved and has a peak flux of 54.9 mJy/beam (contour levels in mJy per synthesised beam are 55, 40, 30, 20, 10, 5, 2.5, 1, 0.75).
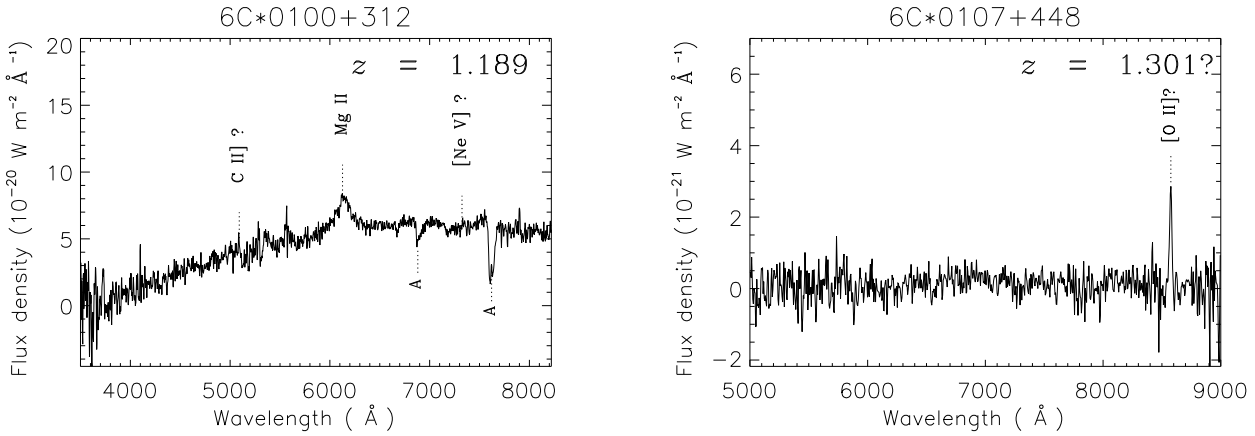

Figure 13: Spectra of two of the sources excluded from the 6C* sample on account of their angular size; the absorption bands marked 'A' are atmospheric bands which have not been fully removed from the data. 6C*0100+312 (left) is a quasar with a broad line most plausibly associated with MgIIλ2799 Å (FWHM = 133 $\pm$ 21 Å and flux = 3.9$\times$10^{-18} W m^{-2} $\pm$ 20%) at $z = 1.189$. This spectrum was taken at the WHT on the 1995 observing run with an integration time of 500 seconds with a slit width of 3.2 arcsec; the PA of the slit was 160° to align with the radio structure. 6C*0107+448 (right) is a spectra of what is possibly emission from the hotspot of this large classical double. The identification of the emission line at 8575 Å is undetermined, but could plausibly be [OII] at $z = 1.301$.
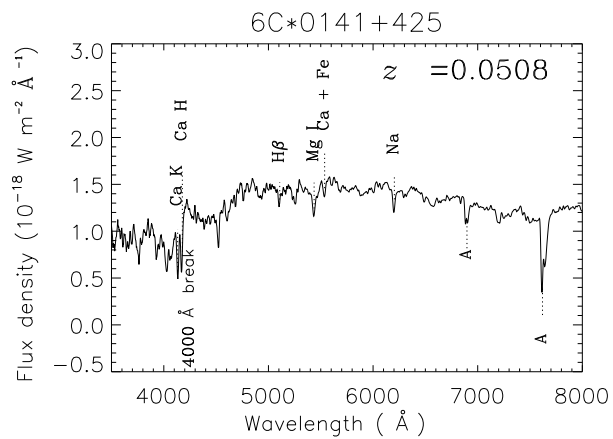
Figure 14: 6C*0141+425 (right) is a galaxy at $z = 0.0508$ with the spectrum dominated by stellar absorption features. This spectrum was taken at the Lick-3m telescope in 1998 with an integration time of 1200 seconds and a slit width of 2.0 arcsec.